# *Student Friendly Guide*
## *to the*
# Cosmic Microwave Background

Robert D. Klauber

www.quantumfieldtheory.info

July 25, 2015(original) Latest revision: November 10, 2025

## Abstract

This document provides what is hopefully a relatively easy-to-understand introduction, suitable for someone with undergraduate physics training, to the power spectral analysis of the cosmic microwave background (CMB), as unveiled by the COBE, WMAP, Planck and other experiments of in recent decades. It proceeds step-by-small-step at a moderate (by physics standards) level of mathematical sophistication and can serve as a simplified initial foundation for those wishing to enter the field, or for others who simply desire a more in-depth understanding of the CMB than the online popular accounts offer. It is halfway between those online popularizations and typical cosmology textbooks.

## Full disclosure

I am not a researcher/expert in this topic, but feel I can offer a fair pedagogic introduction to some areas of the subject for others like me who have physics backgrounds, but are not working in the field. Suggestions and corrections are always welcome via the feedback link on the home page above (which also contains links to pedagogic treatments of other physics topics).

RDK

## Two Parts to This Document

This document is divided into two main parts, the basic introduction and the appendices. The basic material covers the physical mechanisms giving rise to the cosmic microwave background (CMB) and how we analyze the CMB using spherical harmonics. The appendices provide a fairly in-depth development of spherical harmonic analysis and power spectral analysis, for those not completely at home with them. The first part comprises 26 pages; the appendices, 17 pages.

## Table of Contents

# 1 The Cosmic Microwave Background Power Spectrum

If you are reading this, you have no doubt seen the diagram of Fig. 1. It shows the now famous cosmic microwave background (CMB) power spectral analysis of temperature variations across our sky. In this document, I try to present an introduction to it (where it comes from, what is the math behind it, and what it means) that is reasonably transparent to anyone with an undergraduate background in physics.

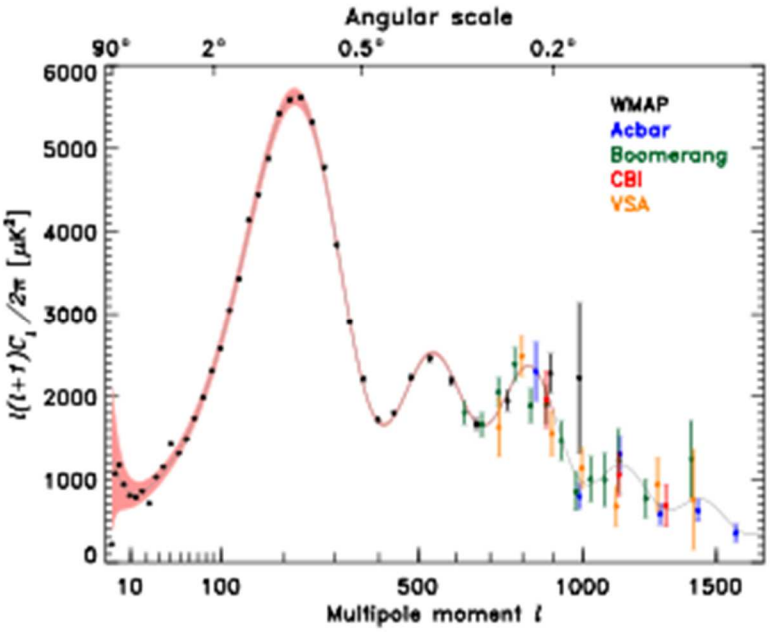


**Figure 1. Power Spectrum of the Cosmic Microwave Background Radiation (CMBR) Variations**

# 2 Spatial Temperature Variations from Early Quantum Variations

In this section, we overview where the temperature variations of the CMB come from.

## 2.1 Density Wave Oscillations from Quantum Variations

Tiny spatial variations in one or more quantum fields at the beginning of inflation lead to spatial variations in mass-energy density. These variations grow to macroscopic scales during inflation and the subsequent expansion of the universe. Such variations comprise regions of greater mass-energy density and regions of lesser mass-energy density. The denser regions attract other matter and initially the dense regions grow denser and the rarefied regions grow more rarefied. This process would simply continue except that a pressure develops in the denser regions that begins to repel the matter moving toward them. The pressure arises as follows.

For the first 380,000 or so years after the big bang, temperature was so high that atoms could not form, and the universe consisted of a "soup" (a plasma really) of charged particles (primarily protons and electrons) interacting with one another. The most significant interactions were electromagnetic ones between charged baryons and photons, which were continually and frenetically bouncing off one another. Thus, the photons exerted a pressure on the baryons. If mass-energy were distributed completely evenly, the pressure, as in a static perfect fluid, would be the same everywhere.

However, as a denser region attracts mass from the surrounding less dense regions, the e/m interactions in the denser region increase, thus increasing the photon pressure in that region. This pressure builds until it ultimately repels the incoming mass and causes it to rebound. The rebounding mass forms density variation waves that propagate.

The ensuing process parallels that of a spring-mass system, which we review in the following section.

Note that both electrons and baryons are in the charged matter mix, but an electron is 1/1,836 of the mass of a baryon, so electrons contribute little in the way of inertia to the dynamics, and can be safely ignored. The electrons are but slaves to baryonic motion. Hence, when we talk of normal (standard model, not dark matter) mass-energy herein, we will effectively mean baryons and photons.

## 2.2 Spring-Mass Oscillations: A Parallel of the Early Universe

The top half of Fig. 2 shows a spring mass system initially in a static state with no gravity acting and the spring unstretched and uncompressed. We then imagine gravity kicking in, and the mass starts moving downward. The spring compresses more, and via Hooke's law, the force in it increases. When the spring force and gravity force are equal, the mass has downward velocity, so it doesn't stop, but keeps moving downward. But, the spring force increases, so the net force is upward, and the mass decelerates, until it stops, then reverses direction and starts moving upward. The spring force then gets less and

less, but when it equals the gravity force, the mass has upward velocity so it keeps going. Then, the gravity force is greater than the spring force, so the mass slows down until it stops, and reverses direction. And the process repeats.

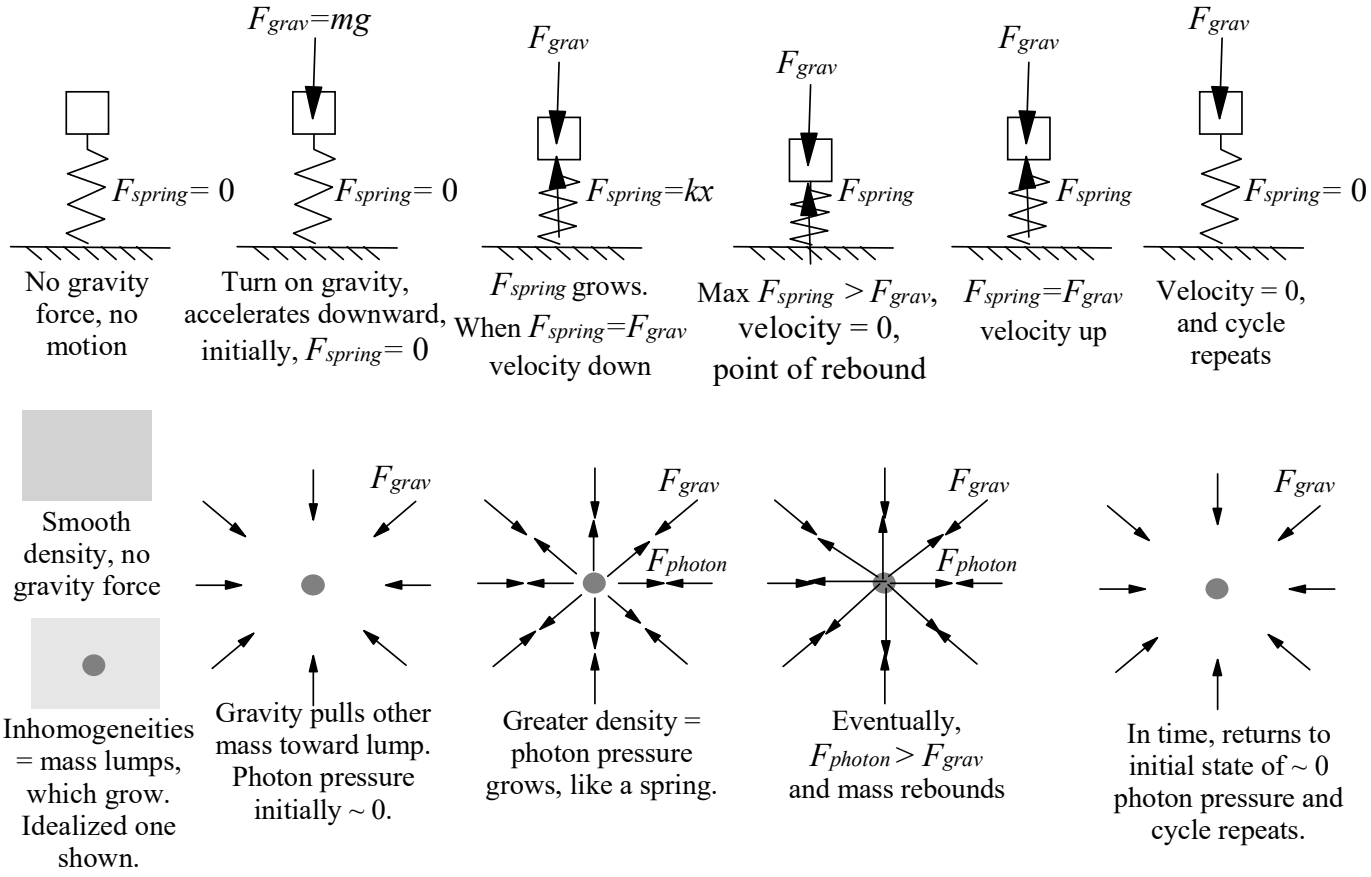


**Figure. 2 Spring-Mass Oscillations Analogous to Pressure Waves Oscillations**

## 2.3 Density Wave Oscillations

This is similar to what happens with density and pressure variations in the early universe, as illustrated in the bottom half of Fig. 2.

If the universe's mass-energy density were 100% smooth, nothing would happen, similar to the static spring mass case we showed with no gravity. But, with inhomogeneities, some regions have higher density than others, which we can think of as "lumps" of mass-energy, and those lumps attract the other matter around them.

So, the surrounding matter is initially pulled inward, toward the center of the lump. But, then the photon pressure increases, like the spring force did with the mass compressing it, until eventually the photon pressure outmatches the gravity force, and subsequently, the (baryonic) matter starts being pushed back outward.

As the matter gets further from the center, the photon pressure on it decreases, until the gravity force then outmatches it. The outward flow of matter slows down, eventually stops, then starts getting pulled inward again. If nothing intervened, the cycle would simply repeat, over and over, as density waves moving inward and outward.

## 2.4 Pressure (Acoustic = Sound) Waves from Density Waves

Where density is higher, so is pressure. And sound waves are simply pressure waves. So, we can think of these waves as density, or pressure, or sound waves, as we like.

For the sound (acoustic) waves we usually consider, the pressure is due to gas molecules interacting with other gas molecules, not photons. With everyday sound waves, high and low density regions propagate due to the pressure variations between those regions. The speed of those waves for an ideal gas (which the plasma approximates) is

$$c_{sound} = k\sqrt{p / \rho} \tag{1}$$

where $p$ is pressure, $\rho$ is density, and $k$ is an appropriate constant depending on the system of units employed.

As it turns out, the baryon-photon plasma does not generate sound waves that all have the same wavelength, but rather a whole spectrum (all different wavelengths) of essentially acoustic waves propagating through it in all directions.

As we will see, these sound waves interact with one another, destructively interfering in some regions and forming standing waves, via constructive interference, in others. These standing waves are called baryonic acoustic oscillations (BAOs).

### 2.5 Temperature Waves from Pressure (Acoustic) Waves

Wherever the density waves are denser, the pressure is higher. Higher pressure means hotter baryons (moving faster = higher energy). In interactions with photons, the baryons would impart more energy to the photons, resulting in higher frequency light emanating from the denser regions. Measuring the light frequency at a given point in space would then be equivalent to measuring temperature at that point.

In short, for a local region of baryons,

$$\text{higher } \rho \rightarrow \text{ higher } p \rightarrow \text{ higher } T \rightarrow \text{ higher frequency of } \gamma \text{ scattered.}$$

## 3 Freezing the Temperature (Photon Frequency) Patterns

### 3.1 Recombination and the CMBR Today

At around 380,000 years after the big bang, average temperature of the universe had fallen to the point where baryons could capture electrons and form atoms (mostly protons and electrons to form hydrogen, but small amounts of helium and lithium atoms were also formed.) This point in time is, strangely enough, called recombination, even though it was the first time particles combined to form atoms, not a "recombining", which implies it had happened before. (And some think physics can be confusing….) This naming is due to a historical misunderstanding of earlier epochs. A better name would be "decoupling", or just "combination".

Once recombination occurred, there was no longer a charged baryonic plasma scattering photons wildly and regularly. The atoms, with exceptions so rare as to not matter, did not scatter the photons, so the photons were effectively released from their electromagnetic bondage to baryonic matter. The photons streamed forth and spread outward through the rest of the universe.

The key point is that at that moment ("cosmic" moment), the photon frequencies reflected the temperatures of the local regions they last were in contact with. These frequencies were, in effect, "locked in" until the present day. Those variations in frequency are what COBE, WMAP, Planck, and other experiments have recently measured. That, including the average background temperature/frequency are what we see today as the cosmic microwave background radiation (CMBR).

Note however, that due to the expansion of the universe since recombination, the frequencies of all photons have been reduced (wavelength stretched by expansion). This is taken into account when the photon frequencies data is analyzed. The relative differences remain as all photons are stretched by the same ratio by cosmic expansion (subject to some subtleties that we won't get into).

The universe has expanded (in a linear direction) by a factor of about 1100 since recombination. This means the average distance between CMBR photons, which was about 1 cm upon release, is now about 11 meters. It also means the originally hot (short wavelength) photons are now much colder (longer wavelengths), such that the average temperature today of the CMBR is $2.725^{\circ}$ K. Variations about that, due to inhomogeneities at recombination, are on the order of 1 part in $10^5$, and these variations about the mean are what is plotted in Fig. 1 on the vertical axis.

The CMB today makes up 99.75% of all photons in the universe. Without the expansion of the universe to cause the cooling of the CMB, the night sky would shine as brightly as the Sun.

### 3.2 An Important Number: The Distance Sound Travels Up to Recombination

An important number in all the CMBR calculations is the distance sound can travel in the 380,000 years from the big bang to recombination. We label this distance herein as $L$.

We can think heuristically of $L = (c_{sound})(t_{recomb})$, where $t_{recomb}$ = 380,000 years in appropriate units, but note that due to pressure and density changes as the universe evolves, $c_{sound}$ varies over time, so we would need to integrate to find $L$, rather than use a simple multiplication. Additionally, the universe continually expands, so any length one might determine at one point in time gets stretched at later times. Cosmologists can readily make the appropriate calculations to find $L$.

## 4 Density/Pressure/Temperature Wave Patterns

### 4.1 Modeling the Waves

The original wave formations of Fig. 2 can be described, for a single higher density lump, in a spherical coordinate system with origin at the center of the lump, and with a separate such system for each lump. But then, when analyzed over the entire

universe, a single Cartesian system is easier and more appropriate. Yet, when viewed from the Earth, the sky appears spherical, so a spherical system centered on the Earth is, by far, the easiest.

So, for our mathematical expressions of the waves, we need to be able to transform between three sets of coordinate systems.

1. A large number of local spherical systems, one for each set of waves originating from a "lump"
2. A single Cartesian system for all waves in the whole universe.
3. A spherical system from which we view those waves from Earth.

Additionally, our final results (as plotted, for example, in Fig. 1) will be statistical averages, with appropriate confidence levels. We will need to find average wavelengths, and amplitudes, of waves, for example, over many lumps.

### 4.2 Phases of Different Modes at Recombination

Note that the spherical waves of coordinate system #1 above can be modeled as a Fourier series of plane waves in Cartesian coordinates. That is, any wave of any form, even spherical, can be modeled as a sum of sine and cosine terms in an x-y-z coordinate system. We employ that x-y-z system in what follows. In this context, it is also relevant that waves formed around a lump are not specifically spherical anyway, as density varies in any number of ways around the lump. In one particular direction it may be greater, or more varied, than in another direction. So, the local Cartesian system can serve us well, and in the process, make it an easy jump to the single universal Cartesian coordinate system #2 above.

It turns out that the density oscillations form standing waves, rather than the traveling waves one might naively expect. Fig. 3 can help in illustrating how this works.

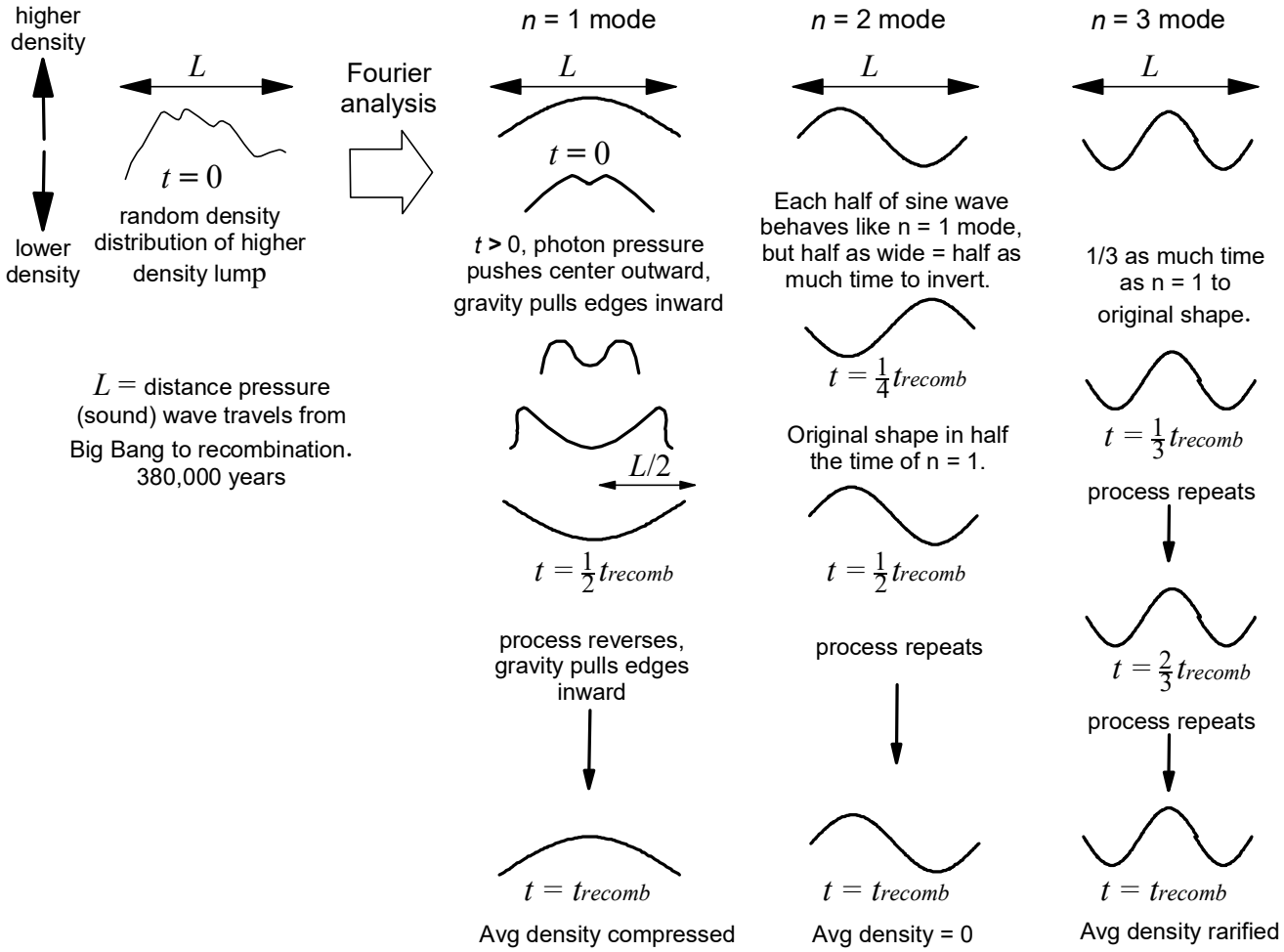


**Figure 3. Evolution of the First Three Standing Wave Modes to Recombination Time**

In the top left part of Fig. 3, we depict a density variation over the length $L$ (the distance sound/pressure waves travel in 380,000 years), where $L$ has been chosen for reasons that should become apparent. The center of the variation is effectively the center of a "lump" of matter that is denser than its surroundings. The time $t = 0$ means at the end of inflation. The pattern of the density variation is random and will vary from place to place, so the top left diagram shown is only one of many possible ones.

To the right of that, we show a Fourier breakdown of the first three Fourier wavelength modes. An infinite number of such modes, in principle, sum to comprise the overall density variation shown on the left. We consider the spatial origin at the center of the density lump, so the $n = 1$ mode is a cosine wave around $x = 0$, $n = 2$ is a sine wave, $n = 3$ a cosine wave, etc.

Consider how the $n = 1$ mode evolves over time. At the center, density is high, so photon pressure is high, and it repels the matter there, in two opposite directions. Each density bump shown moves at the speed of sound, $c_{sound}$, and the distance to the edge in the figure is $L/2$. So, it takes the lumps half of 380,000 years to each reach the edge.

At that point, when photon pressure has diminished, the force of gravity pulls the two dense edges back to the center. Since these higher density regions travel at $c_{sound}$, it takes them half of 380,000 years to cover the distance $L/2$ back to the center. So, after 380,000 years, the first mode has cycled once and returned to its original shape.

How about the $n = 2$ mode? Well, it essentially is composed of a wave like the $n = 1$ wave at $t = 0$ on the left but only $L/2$ wide, instead of $L$ wide, plus an $n = 1$ mode wave at $t = 0$ and $L/2$ wide on the right. These behave like the $n = 1$ mode did, except the distance the density variations (humps in the diagrams) only have to travel half as far, before turning around. Thus, it takes the $n = 2$ mode half as long as the $n = 1$ mode to invert and half as long to return to its original form. So, it cycles twice in 380,000 years, but at the end of that time, it looks like it started.

Note that when we say "looks like it started" we mean it has the same general shape. Since the universe has been expanding over 380,000 years, the wave length and amplitude will be stretched by the expansion. So, it has the same shape, but not the same dimensions.

The $n = 3$ mode cycles three times over 380,000 years, as can be gleaned from the far right part of Fig. 3. In general, the number of cycles of each mode, from the end of inflation until recombination, equals the mode number $n$.

Importantly, for each mode of waves specifically extending over length $L$, we have standing (not propagating) waves. They stay in one place, oscillating up and down, and at recombination time have a specific cosine or sine form.

The wavelengths of the various modes are $\lambda_n = \lambda_1/n$, where $\lambda_1 = 2L$. The frequencies of oscillation are $f_n = nf_1$. All else being equal, the standing waves of wavelengths $\lambda_n$ would be spread randomly across the universe at different amplitudes and in different directions, and that's where statistics come in (to be discussed later).

### 4.3 Character of the Standing Waves

Note that the fundamental ($n = 1$) mode is compressive. The wave represents higher density (and thus higher pressure and temperature). The $n = 2$ mode is half compressive (higher density) and half rarified (lower density, expanded), so in net overall, it is neither compressive nor rarified. The $n = 3$ mode is two parts rarified, and one part compressive, so, in net, it is rarified.

In general, the even numbered modes, which are sine waves, will have net zero density variation (integrated over the whole wave). Odd number modes, which are cosine waves, will be alternately compressive and rarified. $n = 1, 5, 9, \ldots$ are compressive. $n = 3, 7, 11, \ldots$ are rarified.

In part, for the above reason, the sine modes play little role in the CMBR, as it is concerned with waves exhibiting compression or rarefication. There is yet another reason why the sine modes have little impact on calculations or observations. For every sine mode at $t = 0$, having the shape ∿ , there is another with shape ∩ . When we add them all together, over large numbers, they all cancel. The cosine waves, on the other hand, have to be predominantly higher density in the center (not lower, i.e., not below the horizontal centerline of the waves), because the original random density variation was a higher density lump. The cosine waves contribute overall. The sine waves do not.

### 4.4 Waves Other than *L* in Length

We have restricted the above discussion to waves fitting exactly inside the distance $L$. How about other waves of different wavelengths?

They, it turns out, do not form standing waves, like those of Fig. 3. For example, half cosine waves like our $n = 1$ mode diagram with length $> L$, do not have enough time before recombination to return to their original form. Waves with length $< L$, will at recombination time, not have returned precisely to their original form, but gone beyond that to some intermediate state.

Large numbers of these waves interfere, constructively in some places, destructively in others. But over large numbers of random superpositions of waves of various wavelengths, they essentially cancel out, netting zero effect.

Bottom line: Only the odd numbered modes of wavelength $2L/n$ contribute to any degree to the CMBR. Of these, the $n = 1, 5, 9, \ldots$ modes are compressive, the $n = 3, 7, 11, \ldots$ modes are rarified.

### 4.5 Phases of the Various Acoustic Waves

Note that all the wave formations started at the same time. So, for example, all of the various fundamental modes ($n$ = 1 in Fig. 3) distributed throughout the universe would have their corresponding humps begin to propagate at the same time. They all propagate at the same speed and are subject to the same dynamics. So, the many different fundamental standing waves set up all over the universe would all be in phase in time and remain so as time progresses. Every $n$ = 1 mode, everywhere in the universe would return to its original shape in 380,000 years.

Ditto for higher modes. Hence, all standing waves throughout the universe having the same wavelength remain in phase in time, i.e., all standing waves having the same mode number $n$ peak at the same time.

## 5 The Last Scattering Surface

For us, as we look out into the universe, we look into the past, due to the great distances light must travel to reach us over the history of the universe. Looking in any direction, the light from recombination (CMB) reaches us from the same distance away, from all directions, at the same time. Thus, it is effectively coming, from our perspective, from a vast shell at a distance all but several hundred thousand light years from the edge of the visible universe. Hence, that shell looks to us like the surface of a giant sphere.

Since this spherical shell represents the last light to be scattered from primordial free baryons, it is called the last scattering surface (LSS).

The modes of Fig. 3, and higher modes, we see now are those from the LSS. But the LSS is best treated in a spherical coordinate system centered on the Earth, and we have been working with waves in a Cartesian system. Sects. 7 and 8 show how we go from that Cartesian system to the spherical system in which our measurement of the CMB is carried out.

## 6 Points to Note about Waves

### 6.1 Three Kinds of Waves

We typically think of waves as propagating through space, like water waves, sound waves, or electromagnetic waves. But waves can also be non-propagating, yet oscillating back and forth, like a guitar string when plucked or a string tied tightly between two walls and pulled for a moment in one direction. As you learned in freshman physics, this latter type of wave is known as a standing wave.

There is yet a third kind of wave, which some may not consider a real wave, but which is relevant for us. This is a wave shape in space that does not propagate, and also does not oscillate back and forth, such as the old washboards used in the early 1900s, or the ripples one sees on many dirt roads. These oscillate in space, but not in time. We will call such waves frozen waves. See Fig. 4.

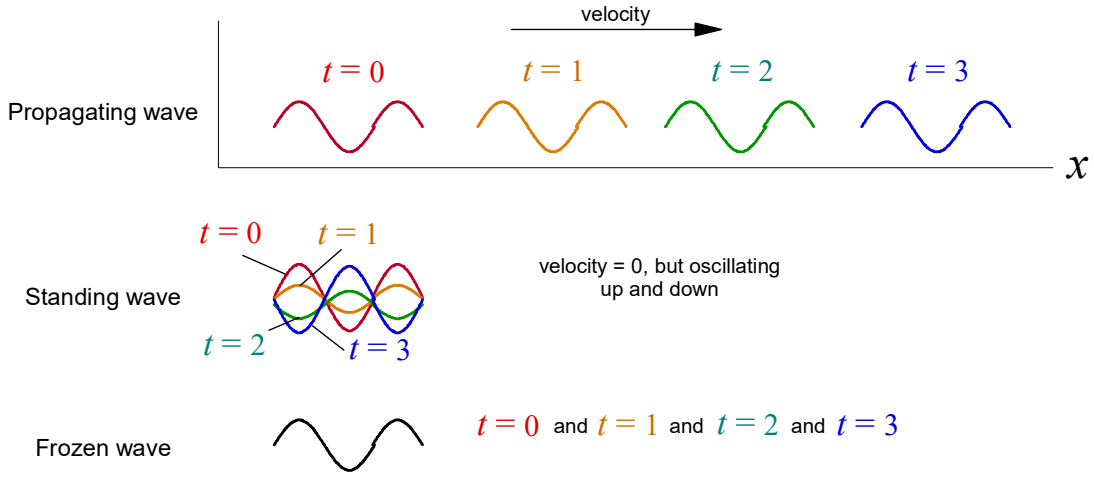


**Figure 4. Three Different Kinds of Sinusoidal Waves**

### 6.2 Two Different Materials for Wavelengths in CMBR Analysis

Don't confuse the wavelengths of density/pressure/temperature waves with the wavelengths of the photons that are released at recombination. The temperature variations form waves with high temperature in some places and low in others. The photon wavelengths released at any of the various points along the temperature wave are indicators of the matter temperature at that point.

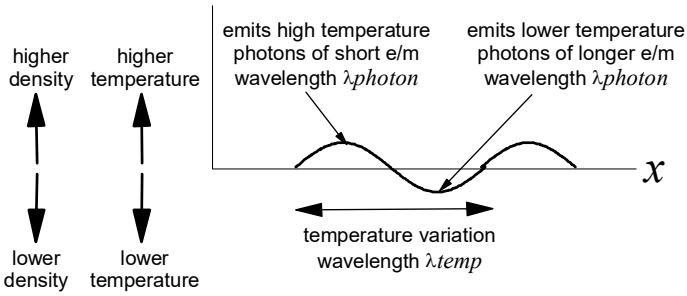


**Figure 5. Distinction between Temperature Wave Wavelengths and Photon Wave Wavelengths**

### 6.3 CMBR Type Waves

Density/pressure/acoustic/temperature waves prior to recombination are mostly propagating waves (moving with the speed of sound), but some of these waves form standing waves, in the manner shown in Fig. 3. The temperature waves (of Fig. 5) from recombination on, however, are reflected in the frequencies of the myriads of photons released (as in Fig. 5) at that time. These temperature waves are patterns, literally in the sky, and these patterns are locked in (but for minor effects) over billions of years, until we see them today much like they were at recombination. The temperature wave patterns are frozen. They have oscillations in space, but not in time.

### 6.4 Gleaning Information from the Wave Patterns

The characteristics of the acoustic/temperature/photon waves depend on things like photon density, normal matter density, dark matter density, the speed of sound, the strength of gravity, the strength of the electromagnetic interaction, the percentages of normal matter vs dark matter, and (if any existed) interactions between normal and dark matter. Temperature wavelengths detected and amplitudes of each mode are functions of all of these things.

Additionally, how the amplitudes and wavelengths of the modes change from the time of recombination to the present day, when we measure the CMBR, depends on the rate at which the universe is expanding, the acceleration/deceleration involved in the expansion, and the curvature of the universe. If dark energy is accelerating the expansion, then the waves change in ways reflecting that acceleration. And that, in fact, is one of the key results of the CMBR analysis. It confirms the supernovae research finding of dark energy.

To visualize, in one instance, how these different factors may come into play, consider the interplay between photon pressure and matter (both normal [baryonic] and dark).

A local higher density inhomogeneity, which we have been calling a "lump", attracts the surrounding matter, both baryonic and dark, as both matter types interact gravitationally. As they fall inward toward the center, photon pressure builds up, but that pressure only affects baryonic matter, not dark matter, as it (at least to very high degree) does not interact electromagnetically. So, the rebound effect of photon pressure eventually causes the baryonic matter to reverse direction and start moving back outward again. But, the dark matter is not affected by this pressure, so it keeps moving inward, attracted by gravity. However, the normal matter moving back outward affects the dark matter gravitationally and so, modifies its motion.

It is not hard to recognize that the characteristics of the CMBR waves will be different for different ratios of dark to normal matter. The math behind all of this is extensive and complicated, but it does, clearly and specifically, prescribe what the CMBR patterns we measure today can tell us about the percentages of dark and normal matter that exist in our universe.

We will look a little more closely at all of this in Sect. 12.

## 7 Plane Standing Waves in a Spherical Analysis

### 7.1 Graphically for Simplified Case

Consider one plane wave of the fundamental baryon acoustic (sound/pressure) mode (as $n = 1$ in Fig. 3). Pretend, for the sake of this discussion, that at the time of recombination, the wave extends in its direction of travel across the universe. That is, over each length $L$, the fundamental standing wave is repeated. Things are actually far more diverse than this with various modes overlapping in various directions all over the place. However, we simplify here to make a point. We represent this simplification in Fig. 6.

Fig. 6 is almost self-explanatory. The fundamental wave of the figure is frozen after recombination. The baryons were most compressed at the peaks right before recombination, so photons that emanated from those regions are hottest (higher frequency). The nodal regions were not so compressed, and the photons from those are colder (lower frequency).

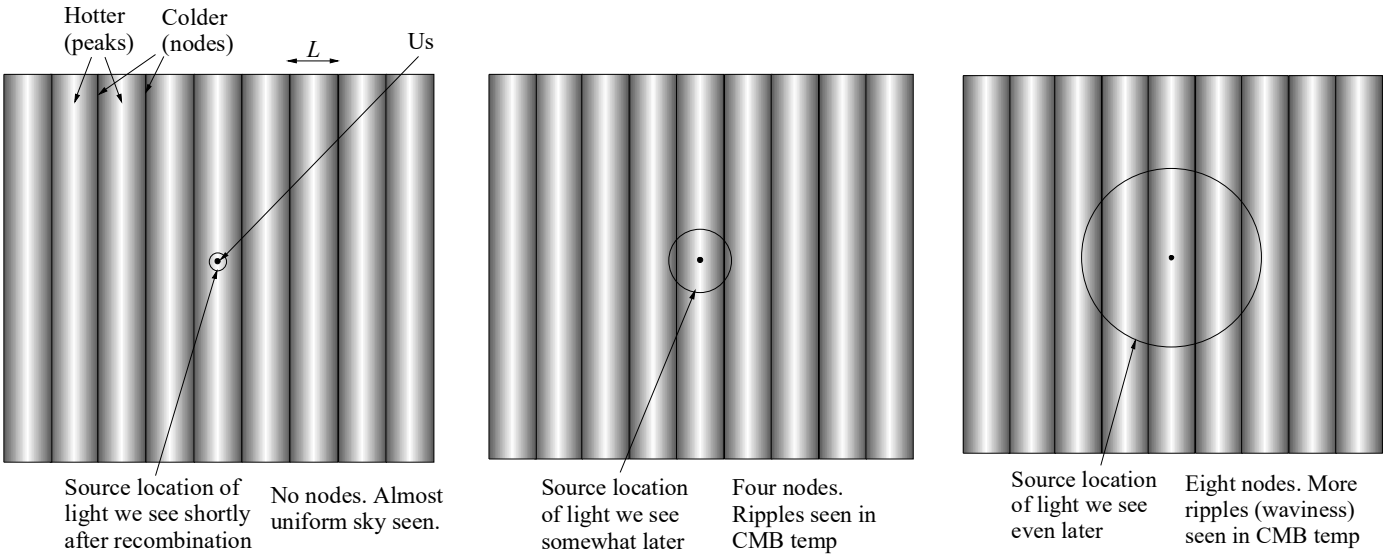


**Figure 6. Over Time, Plane Waves Appear As Higher and Higher Modes on Sphere from which Light Reaching Us Left**

Just after recombination (left most part of Fig. 6) light from the time of recombination had not traveled very far to reach us, so we can't yet see much variation in temperature of the photons reaching us. Somewhat later (middle part of Fig. 6), the light reaching us from that time is from further away, so we start to see some nodes. At a later time, we would see more nodes, as in the righthand part of Fig. 6. As time goes on, we would see more and more nodes (higher modes) appearing on the spherical shell of the last scattering surface (LSS).

Note that if the middle figure were just a bit earlier, with the circle just touching the dark lines (nodal lines), we would see a quadrupole (2 colder regions and 2 hotter regions in 360°). Higher and higher *n*-poles appear as time goes on. At the present time, a fundamental standing wave from recombination of the ideal wave shown in Fig. 6 (which is not the case in nature) would appear to us to have hundreds of nodes, spaced a little less than one degree apart.

## 7.2 The Real, Not Ideal, Case

Of course, we don't have the ideal situation as in Fig. 6, where a single wave form repeats itself perfectly, over and over, across the universe. What we actually have are a whole slew of small waves of various lengths between humps (see Fig. 3) all over the place, depicted schematically in Fig. 7.

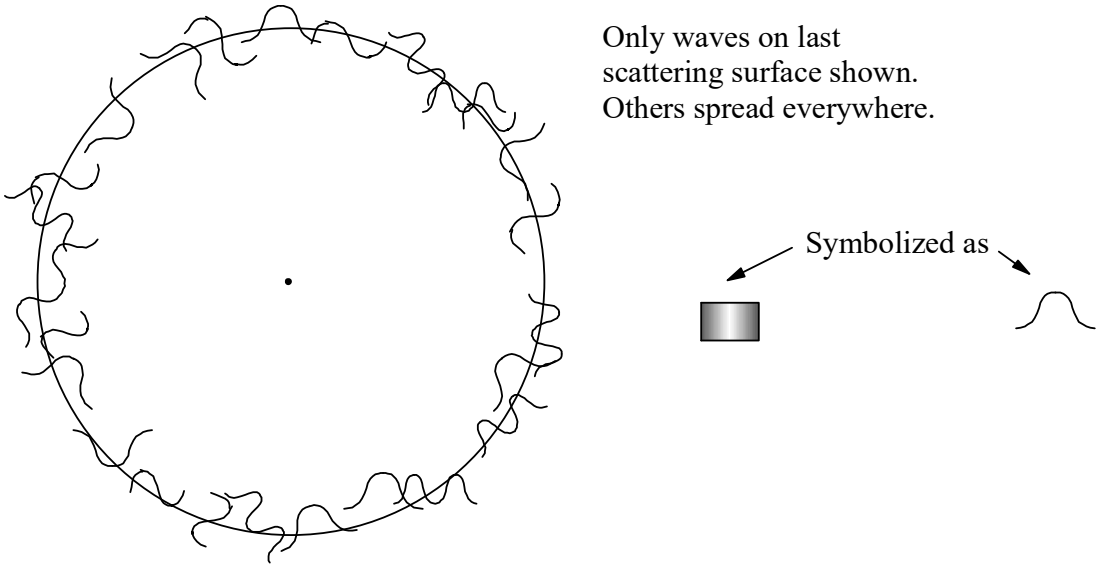


**Figure 7. Some Local Temperature Standing Waves on Last Scattering Surface (Only lower modes shown)**

For a local fundamental wave (one hump, $n = 1$) the space between nodes at our present time is a little less than one 1°.

### 7.3 Converting Plane Waves to Spherical Coordinates

Because a plane wave, such as those of Figs. 3, 4, and 5, appears to us as ripples on a spherical surface, our preferred method of analyzing data from those ripples is with a spherical coordinate system. To do that, one needs to convert a plane wave expressed in Cartesian coordinates (which is the easiest way to express a plane wave) into spherical coordinates centered on the Earth. This is done via a mathematical relation known as Rayleigh's plane wave expansion, which we will present after discussing spherical harmonics in Sect. 8.

## 8 Spherical Harmonic Analysis

### 8.1 Background

Our data is a map of the temperature variations of the cosmic microwave background (CMB) radiation in the sky and thus, is taken effectively over a spherical shell. So, if we want to break down the temperature signal we see via a modal analysis, it is best to use the spherical analog of a Fourier spectral analysis, i.e., spherical harmonic spectral analysis. The central concept behind spherical harmonic analysis is explained briefly in Wholeness Chart 1 (next page) and the following paragraphs, with a more in-depth treatment in Appendix A.

**Bottom line** Spherical harmonics are the spatial part of the solutions to the wave equation in spherical coordinates, just as sines and cosines (or exponentials, $e^{ix} = \cos x + i \sin x$ ) are its spatial solutions in Cartesian coordinates.

A spherical harmonic series parallels the Fourier series, but we use spherical coordinates $\theta$ and $\phi$. rather than Cartesian ones. For the CMBR, we consider $r$ fixed, so the analysis is effectively over the surface of a sphere, where only $\theta$ and $\phi$ vary.

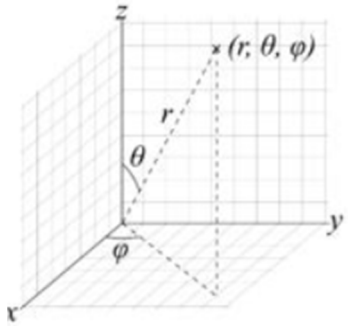


**Figure 8. Spherical Coordinates**

$$f(\theta,\phi)=\sum_{l=0}^{\infty}\sum_{m=-l}^{l} a_{lm}Y_{lm}(\theta,\phi) \qquad \left(\begin{array}{l} Y_{lm}(\theta,\phi) \text{ and } a_{lm} \text{ are generally complex, though they} \\ \text{can result in a real function } f(\theta,\phi), \text{ as in our case.}\end{array}\right) \tag{2}$$

$$\text{similar to } f(x)=\sum_{n=0}^{\infty} A_n(\cos nkx + i\sin nkx)=\sum_{n=0}^{\infty} A_n e^{inkx}$$

$$\text{or in flat 2D, } f(x,y)=\sum_{n_x=0}^{\infty}\sum_{n_y=0}^{\infty} \underbrace{A_{n_xn_y}}_{\substack{\text{analogous}\\ \text{to } a_{lm}}} \underbrace{(\cos n_x kx + i\sin n_x kx)(\cos n_y ky + i\sin n_y ky)}_{\text{analogous to } Y_{lm}(\theta,\phi)} = \sum_{n_x=0}^{\infty}\sum_{n_y=0}^{\infty} A_{n_xn_y} e^{in_x kx} e^{in_y ky} \tag{3}$$

Unfortunately, the spherical harmonics $Y_{lm}(\theta,\phi)$ are not of as simple a form as the sines and cosines of the linear dimension case. (See Appendix A for an extensive development of spherical harmonics. They are virtually impossible to display graphically because they are complex numbers, but Fig. A-3 of Sect. 15.5, pg. 34, graphs the absolute values of those complex numbers for $l$ = 0,1,2.) However, just as the Fourier components (the harmonics, one for each $n$ value in 1D) are mathematically orthogonal over a given spatial interval, the spherical harmonics $Y_{lm}(\theta,\phi)$ are mutually orthogonal on the surface of a sphere (over the intervals $0 < \theta < \pi$ and $0 < \phi < 2\pi$).

(2) is what is used in quantum mechanics for the hydrogen atom solution to the Schrödinger equation in spherical coordinates, so you have probably seen a relation like this before (with a complex wave function $\psi$, rather than a real $f$ ). Each $a_{lm}$ represents the amplitude of a particular spherical harmonic component in the summation. In the hydrogen atom we were also concerned about the $r$ direction and had a separate solution which was only a function of $r$ (the Schrödinger equation was separable into a purely $r$ dependent part and a part dependent on $\theta$ and $\phi$. Here we ignore the $r$ dependence since we are only concerned with describing a function [the temperature variations] of angular location, i.e., effectively on the surface of a sphere.)

**Wholeness Chart 1. Wave Equation in Cartesian and Spherical Coordinates**

Wave equation $\frac{\partial^2}{\partial t^2} f - v^2 \frac{\partial^2}{\partial x^2} f = 0 \quad \xrightarrow{3D} \quad \nabla^2 f - \frac{1}{v^2} \ddot{f} = 0$

| | **Cartesian** | **Spherical** |
|---|---|---|
| Indep vars | $f = f(x,y,z,t)$ | $f = f(r,\theta,\phi,t)$ |
| Laplacian operator | $\nabla^2 = \frac{\partial^2}{\partial x^2} + \frac{\partial^2}{\partial y^2} + \frac{\partial^2}{\partial z^2}$ | $\nabla^2 = \frac{1}{r^2}\left\{\frac{\partial}{\partial r}\left(r^2 \frac{\partial}{\partial r} + \frac{1}{\sin\theta}\frac{\partial}{\partial\theta}\left(\sin\theta \frac{\partial}{\partial\theta}\right) + \frac{1}{\sin^2\theta}\frac{\partial^2}{\partial\phi^2}\right)\right\}$ |
| Solution forms for different Laplacians | $1D \rightarrow f_n(x,t) = \underbrace{B_n \cos n(\omega t - kx) \quad \text{or} \quad D_n \sin n(\omega t - kx)}_{\omega,\, k \text{ for fundamental } (n=1) \text{ mode, } \omega=\omega_1, k=k_1}$<br>$= B_n \cos n\left(2\pi f_{freq}\, t - \frac{2\pi}{\lambda} x\right) \text{ or } D_n \sin n\left(2\pi f_{freq}\, t - \frac{2\pi}{\lambda} x\right)$<br>$= B_n \cos n\left(2\pi \frac{t}{T} - 2\pi \frac{x}{\lambda}\right) \text{ or } D_n \sin n\left(2\pi \frac{t}{T} - 2\pi \frac{x}{\lambda}\right)$<br>$f_n = A_n e^{in(\omega t - kx)} = B_n \cos n(\omega t - kx) + iD_n \sin n(\omega t - kx)$ | $3D \rightarrow f_{klm}(r,\theta,\phi,t) = a_{lm} j_l(kr) Y_{lm}(\theta,\phi) g(t)$<br>$j_l(kr) =$ spherical Bessel functions<br>$\underbrace{Y_{lm}(\theta,\phi)}_{\text{spherical harmonics}} = \sqrt{\frac{2l+1}{2}\frac{(l-m)!}{(l+m)!}} \underbrace{P_{lm}(\cos\theta)}_{\text{Legendre polynomials}} \frac{e^{im\phi}}{\sqrt{2\pi}}$ no sum $l$, $m$<br>$g_n(t) = e^{\pm in(\omega t)}$ |
| General solution | $f = \sum_n A_n e^{in(\omega t - kx)}$ Any wave form $f$ = Fourier series<br>$f(x,t) = \sum_n A_n e^{in(\omega t)} e^{in(-kx)} = \sum_n A_n g_n(t) h(x)$<br>$3D\ (L_x = L_y = L_z) \rightarrow f(x,y,z,t) = \sum_n A_n e^{in\omega t} e^{-in\mathbf{k}\bullet\mathbf{x}}$<br>$= \sum_n A_n e^{in\omega t} e^{-ink_x x} e^{-ink_y y} e^{-ink_z z}$<br>$L_i \text{ diff} \rightarrow \sum_{n_x=-\infty}^{\infty} \sum_{n_y=-\infty}^{\infty} \sum_{n_z=-\infty}^{\infty} A_{n_x n_y n_z} g_{n_i}(t) e^{in_x k_{1x} x} e^{in_y k_{1y} y} e^{in_z k_{1z} z}$ | $f(r,\theta,\phi,t) = \sum_{n=-\infty}^{\infty} \sum_{l=0}^{\infty} \sum_{m=-l}^{l} a_{lm} j_l(kr) Y_{lm}(\theta,\phi) e^{in(\omega t)}$<br>$= \sum_{n=-\infty}^{\infty} \sum_{l=0}^{\infty} \sum_{m=-l}^{l} a_{lm} j_l(kr) Y_{lm}(\theta,\phi) g_n(t)$ |
| Helmholtz equation from wave equation | $\ddot{f} = -\omega^2 f \quad \text{in} \quad \nabla^2 f - \frac{1}{v^2}\ddot{f} = 0 \rightarrow \nabla^2 f + \frac{\omega^2}{v^2} f = 0$<br>$v^2 = \left(f_{freq}\lambda\right)^2 = \left(\frac{\omega}{2\pi}\right)^2 \left(\frac{2\pi}{k}\right)^2 = \frac{\omega^2}{k^2}$<br>$\boxed{\nabla^2 f + k^2 f = 0}$ | Same as at left, but $\nabla^2$ for spherical coordinates<br>$\boxed{\nabla^2 f + k^2 f = 0}$ |
| Checking solution | $\ddot{f} = -\omega^2 f \qquad \nabla^2 f = -k^2 f$<br>$\nabla^2 f - \frac{1}{v^2}\ddot{f} = 0 \quad \rightarrow \quad -k^2 f + \frac{\omega^2}{v^2} f = 0$<br>$v^2 = \left(f_{freq}\lambda\right)^2 = \left(\frac{\omega}{2\pi}\right)^2 \left(\frac{2\pi}{k}\right)^2 = \frac{\omega^2}{k^2}$ | Not trivial with spherical coordinates,<br>but same final result. |
| **Bottom line** | $f(x,y,z,t)$ above is solution to wave eq, Cartesian system | $f(r,\theta.\phi,t)$ above is solution to wave eq, spherical system |
| For fixed $r$ and $t$ | N/A | $f(\theta,\phi) = \sum_{l=0}^{\infty} \sum_{m=-l}^{l} a_{lm} Y_{lm}(\theta,\phi)$ see (2) |
| Finding coefficients | $A_n = \frac{1}{L}\int_{-L/2}^{L/2} f_n^*(x,0) f(x,0) dx = \frac{1}{L}\int_{-L/2}^{L/2} e^{-inkx}\left(\sum A_m e^{imkx}\right) dx$<br>$= \frac{1}{L}\int_{-L/2}^{L/2} A_n e^{-inkx} e^{inkx} dx = \frac{1}{L}\int_{-L/2}^{L/2} A_n dx = \frac{1}{L} L A_n = A_n$ | $a_{lm} = \int_0^{2\pi} \int_0^{\pi} Y_{lm}^*(\theta,\phi) f(\theta,\phi) \sin\theta\, d\theta\, d\phi$ see (4) |

## Wholeness Chart 2. Finding Amplitudes of Fourier and Spherical Harmonic Terms

**Review: Fourier Series in Cosines**

To express $f(x)$ in a Fourier series, we need to know the amplitudes of the sine and cosine terms. For example, for a function we can express in terms of cosines, as in (2-1), we need to know the $A_n$.

$$f(x)=\sum_{n=0}^{\infty} A_n \cos nkx \tag{2-1}$$

To start, we first note that from integral tables,

$$\int_{-L/2}^{L/2}(\cos nkx)(\cos mkx)\,dx=\delta_{mn}\frac{L}{2}\,. \tag{2-2}$$

As an illustrative example of (2-2), consider $n$ = 1 and $m$ = 2. Note from the lefthand figure below how integrating the product of the two yields a positive product some of the time and a negative product the rest of the time. Examination of that figure shows these two contributions to the integral, over the fundamental length $L$, will be of equal magnitude and thus, cancel. We need $m = n$ to get non-zero.

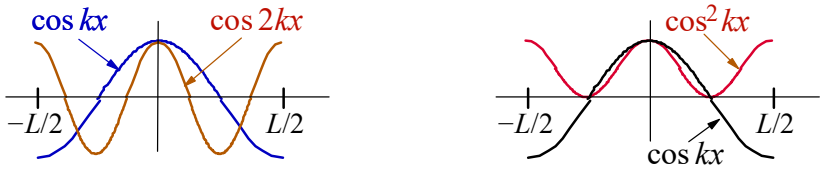


Anything squared is positive everywhere (see righthand figure above), so any integrand of form $\cos^2 nkx$ must yield a positive number. The integral tables tell us that number is $L/2$, as shown on the RHS of (2-2), for any value of $n$.

Note this integral, where we use (2-1) to get the expression after the first equal sign, and (2-2) to get the expression after that.

$$\frac{2}{L}\int_{-L/2}^{L/2}(\cos nkx)\,f(x)\,dx=\frac{2}{L}\int_{-L/2}^{L/2}(\cos nkx)\left(\sum_{m=0}^{\infty} A_m\cos mkx\right)dx=\frac{2}{L}\int_{-L/2}^{L/2}(\cos nkx)\,A_n(\cos nkx)\,dx=\frac{2}{L}A_n\frac{L}{2}=A_n\,. \tag{2-3}$$

Re-arranging the beginning and end of (2-3),

$$A_n=\frac{2}{L}\int_{-L/2}^{L/2}\underbrace{(\cos nkx)}_{\text{or }(\cos nkx)^*}f(x)\,dx\,.\quad\text{Finding the amplitude of any Fourier component in a given } f(x). \tag{2-4}$$

Note: The same thing works if we express $f(x)$ in terms of sines or exponentials. In (2-4), we would have a sine instead of a cosine, or $e^{inkx}$ instead of the cosine. The most general expression of the integrand multiplies $f(x)$ by the complex conjugate of cosine, sine, or exponential, but for real functions like cosine and sine, the complex conjugate equals the original function.

**Spherical Harmonics Series**

Analogous in spherical coordinates to (2-1) in Cartesian coordinates,

$$\underbrace{f(\theta,\phi)}_{\text{like } f(x)}=\sum_{l=0}^{\infty}\sum_{m=-l}^{l}\underbrace{a_{lm}}_{\substack{\text{like}\\ A_n}}\underbrace{Y_{lm}(\theta,\phi)}_{\text{like cos}}\,. \tag{2-5}$$

Analogous to (2-4) is

$$\underbrace{a_{lm}}_{\text{like } A_n}=\int_0^{2\pi}\int_0^{\pi}\underbrace{Y_{lm}^*(\theta,\phi)}_{\text{like cos}^*}\underbrace{f(\theta,\phi)}_{\text{like } f(x)}\underbrace{\sin\theta\,d\theta\,d\phi}_{\text{like } dx}\qquad\text{(4) herein.} \tag{2-6}$$

For

$$f(\theta,\phi)=T(\theta,\phi)\quad\text{found by observation of CMBR temperature,} \tag{2-7}$$

$$\boxed{a_{lm}=\int_0^{2\pi}\int_0^{\pi}Y_{lm}^*(\theta,\phi)T(\theta,\phi)\sin\theta\,d\theta\,d\phi}\quad\text{Amplitude of the } l,m \text{ spherical harmonic in temperature data } T. \tag{2-8}$$

The "$l$" index, an integer, is associated with the number of spatial oscillations (nodes, to be precise, equal to $l + 1$) in the $\theta$ direction in spherical coordinates, and "$m$", the number of spatial oscillations (nodes) in the $\phi$ direction. $m$, also an integer, varies from "$-\ l$" to "$l$" (recall the hydrogen atom). For example, the $l=0$ mode has zero oscillation in the $\theta$ direction, i.e., a monopole, or constant value over the whole sphere, that sets the overall scale. $l=1$ is a dipole: one full oscillation over the sphere in the $\theta$ direction. Go to higher and higher $l$ values, and you get more spatial oscillations (and therefore smaller wavelength) over the sphere surface. The $l$ and $m$ integers of spherical coordinate analysis are analogous to the $n_x$ and $n_y$ integers of (3) for Cartesian coordinate analysis. The $a_{lm}$ are analogous to the Fourier amplitudes $A_{n_x n_y}$ .

## 8.2 Finding the $a_{lm}$

Note that since the $Y_{lm}$ are orthonormal and complete over a sphere at fixed radius $r$ (see Appendix A, Sect. 15.4 pg. 33, summarized in (81) therein) the $a_{lm}$ can be determined (see Wholeness Chart 2 and Sect. 15.6.1 pg .35, eq. (84)) as

$$a_{lm} = \int_0^{2\pi} \int_0^{\pi} Y_{lm}^*(\theta,\phi) f(\theta,\phi) \sin\theta \, d\theta \, d\phi \,. \tag{4}$$

## 8.3 CMB Spherical Harmonics

Note with the CMB that we are dealing with a scalar function over the sphere surface, i.e., the temperature $T$. For us,

$$f(\theta,\phi) = T(\theta,\phi) \tag{5}$$

The $l = 0$ component (zero spatial oscillation) spherical harmonic in (2) is $Y_{00} = 1$, so $a_{00}$ would equal the mean temperature $\overline{T} = 2.725^{\circ}\text{K}$, which is the constant background over the entire sky. The variation from the mean, $\Delta T$, as a function of $\theta$ and $\phi$, are analyzed in terms of its spherical harmonic components $Y_{lm}(\theta,\phi)$ for $l > 0$. Because $T$ is a scalar, there are no issues of what direction our harmonic spatial waves are oscillating in. That is, we don't have to worry about longitudinal vs transverse directions for a scalar. Our temperature waves are scalar waves, so variations are merely numbers.

Key point: If we measure the temperature variation across the sky $T(\theta, \phi)$ [$= f(\theta, \phi)$ in (4)], we can find the amplitude $a_{lm}$ of each spherical harmonic mode via (4).

## 8.4 Expressing Plane Standing Waves in Spherical Coordinates

### 8.4.1 A Simple Complex Sinusoid

The relation alluded to in Sect. 7.3 for expressing a plane standing wave in spherical coordinates is known as Rayleigh's plane wave expansion. (See http://en.wikipedia.org/wiki/Plane_wave_expansion.) We state it here without proof as (6). For a single (complex) sinusoidal wave of unit amplitude with wave vector $\mathbf{k}$ (having wave number $k$ pointing along unit vector $\mathbf{n_k}$, which is completely different from mode number $n$), where $\mathbf{r}$ is the vector from the origin to the point in question (having length $r$ pointing along unit vector $\mathbf{n}$, also different from mode number $n$), where $\theta_{\mathbf{k}}$, $\phi_{\mathbf{k}}$ and $\theta$, $\phi$ are the spherical coordinate angles for $\mathbf{n_k}$ and $\mathbf{n}$, respectively, and where $j_l(kr)$ are spherical Bessel functions,

$$\underbrace{e^{i\mathbf{k}\cdot\mathbf{r}}}_{\substack{\text{coordinate}\\ \text{independent}\\ \text{form}}} = \underbrace{e^{ik_x x} e^{ik_y y} e^{ik_z z}}_{\substack{\text{Cartesian}\\ \text{coordinates}}} = \underbrace{4\pi \sum_{l=0}^{\infty} \sum_{m=-l}^{l} i^l j_l(kr) Y_{lm}^*(\theta_{\mathbf{k}},\phi_{\mathbf{k}}) Y_{lm}(\theta,\phi)}_{\text{spherical coordinates = Rayleigh expansion}} \tag{6}$$

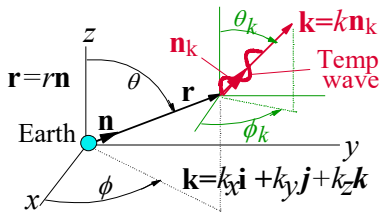


### 8.4.2 Arbitrary Plane Wave Shapes

Any wave shape other than a sinusoid, such as a sum of local waves over the whole sky (Fig. 7, pg. 8), can be expressed, in the spirit of Fourier harmonic analysis, in Cartesian coordinates (bounded by a box $L_x \times L_y \times L_z$ in the discrete solution case) as

$$\underbrace{f(\mathbf{r})}_{\substack{\text{arbitrary}\\ \text{wave form}}} = \underbrace{f(x,y,z)}_{\substack{\text{Cartesian}\\ \text{coordinates}}} \qquad \left(\begin{array}{l} f(\mathbf{r}) \text{ could be temperature pattern at all } \mathbf{r} \text{ (in all of space) at} \\ \text{the present time of the photons scattered at recombination,} \end{array}\right)$$

$$= \sum_{n_x=-\infty}^{\infty} \sum_{n_y=-\infty}^{\infty} \sum_{n_z=-\infty}^{\infty} A_{n_x n_y n_z} \underbrace{e^{in_x k_{1x} x} e^{in_y k_{1y} y} e^{in_z k_{1z} z}}_{\substack{\text{complex sinusoids,}\\ \text{Cartesian coordinates}}} \qquad k_{1x} = \frac{\pi}{L_x} \quad k_{1y} = \frac{\pi}{L_y} \quad k_{1z} = \frac{\pi}{L_z} \tag{7}$$

$$\text{for continuous case} \qquad = \frac{1}{(2\pi)^3} \int A(\mathbf{k}) \overbrace{e^{ik_x x} e^{ik_y y} e^{ik_z z}} \, d^3k = \frac{1}{(2\pi)^3} \int A(\mathbf{k}) e^{i\mathbf{k}\cdot\mathbf{r}} d^3k \,.$$

The same wave shape can be expressed, in the spirit of spherical harmonic analysis, as (see (2) with an additional factor for the radial dependence on $r$, which turns out from math we won't do, to be the spherical Bessel function $j_l$,)

$$\underbrace{f(r,\theta,\phi)}_{\substack{\text{same wave form,}\\ \text{spher coords}}} = \sum_{l=0}^{\infty} \sum_{m=-l}^{l} a_{lm} j_l(kr) Y_{lm}(\theta,\phi) \tag{8}$$

By using (6) in (7) and equating the result to the RHS of (8), one can obtain relationships between the $a_{lm}$ coefficients of spherical harmonic analysis and the $A_{n_x n_y n_z}$ (or $A(\mathbf{k})$) of Cartesian harmonic analysis. We will keep things simple at this point and hold off until Sect. 10 to do this. For now, we simply note the implications of doing so.

Bottom line: If we have a theory developed for standing wave formation in Fourier components in Cartesian coordinates, we can deduce the $a_{lm}$ we would expect to measure for that formation in a spherical coordinate system. If we have data, taken in a spherical coordinate system, we can calculate the $a_{lm}$ for that data. Comparing the two is what is done in analyzing the CMB.

**Wholeness Chart 3. Theoretical and Experimental Approaches to the CMBR**

| **What Used for →** | **Theory** | **When** | **Observation/Experiment** | **← What Used for** |
|---|---|---|---|---|
| QFT & GR | Inflation: Density variations | $t = 10^{-32}$ seconds | | |
| | ↓ | | | |
| QFT, GR, standing wave theory | Density/temp patterns at recombination<br>Cartesian wave analysis | $t$ = 380,000 years | | |
| | ↓ | | | |
| GR, some astrophysics for minor changes | Temp patterns now (essentially unchanged)<br>Cartesian wave analysis | $t$ = 13.8 billion years | Temp patterns now<br> 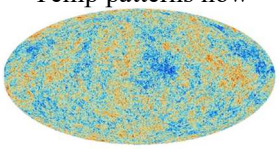 | COBE, WMAP, Planck plus others |
| | ↓ | | ↓ | |
| Rayleigh expansion | Temp patterns now (predicted)<br>Spherical harmonics wave analysis | | Temp patterns now (observed)<br>Spherical harmonics wave analysis | Spherical harmonics math |
| | ↓ | | ↓ | |
| Spherical harmonics math | Plot square of amplitude of each harmonic vs harmonic mode $l$<br>Power spectral analysis (solid line)<br> 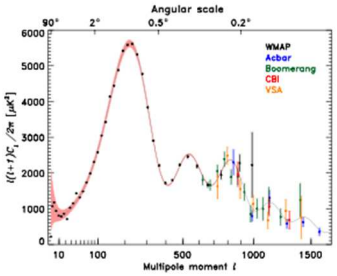 | | Plot square of amplitude of each harmonic vs harmonic mode $l$<br>Power spectral analysis (data dots)<br> 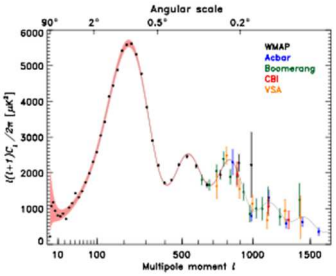 | Spherical harmonics math |
| Note: | Curve depends on amount of normal matter, dark matter, dark energy plus Hubble constant, photon mean free path, inflation spectral density | | Vary parameters at left until theoretical (solid line) curve matches experimental curve (data dots). | |

# 9 Observation: The CMB and the Amplitude $a_{lm}$ of Each Spherical Harmonic $Y_{lm}$

## 9.1 Measuring for the CMB

The spherical harmonics $Y_{lm}$, individually, are not pure sines or cosines, though they are oscillating spatial wave forms. (See Appendix A, pg. 31, eq. (68) for the $\theta$ dependence of several of the lowest modes.) Depicting them graphically is not easy, so we won't do that here, though we show the absolute values $|Y_{lm}|$ for some lower modes in Fig. A-3, pg. 35. Note that the $a_{lm}$ amplitudes of (2) and (4) are analogous to amplitudes of sine waves.

## 9.2 Measuring the CMB Amplitude and Variance

### 9.2.1 Measurement in Our Universe

Recall the CMB radiation displays the acoustic standing wave patterns that existed right at recombination. In other words, we have a cosmic snapshot at one time (recombination), and for any given mode (such as the fundamental with $n = 1$), all localized plane waves everywhere would be in phase in time. (See Fig. 3, pg. 4.) But the heights of the individual standing waves of the same mode would vary from individual wave to individual wave.

As we showed in Sect. 8.4.2, pg. 12, the sum of many plane waves of many modes at many different locations can be represented by spherical harmonics with a given amplitude coefficient $a_{lm}$ associated with each $Y_{lm}$. Thus, the particular $a_{lm}$ we measure would be those at the time of recombination in our universe. In other universes with the same laws but different initial conditions (different random density fluctuations) at their recombination times, we would have different $a_{lm}$. That is, the reds, yellows, blues, and greens in the first figure of the next to last column in Wholeness Chart 3 would be scattered differently. So, the harmonic analysis, i.e., finding the $a_{lm}$, would yield different $a_{lm}$.

### 9.2.2 Measurement Over an Ensemble of Universes

Consider having an ensemble of universes we could collect data from. Each is structured in the same manner as ours, with the same physical laws, particles, and parameters (same curvature, baryon density, dark matter, dark energy, photon density, etc.) However, each has different initial conditions, i.e., random QM variations at the onset of inflation, and these occur randomly throughout members of the ensemble.

If we did have a lot of universes similar to ours and could make many measurements (one in each such universe), a given $a_{lm}$ would vary in value between them. It would be positive in approximately half of them and negative in half, with the average $a_{lm}$ over all universes tending to zero as the number of universes got large. Since our mean value for $a_{lm}$ ($l > 0$) would tend to zero, it is not of great use to us as a characterizing parameter of the CMB. See Fig. 9 for a simplified example, where in the $xy$ plane, the first universe has the 22 mode (like a cosine curve superimposed on the 00 mode) with a positive sign, and the second universe has the 22 mode with the same $a_{22}$ magnitude, but opposite sign. The 22 modes cancel.

Cross sections of certain modes

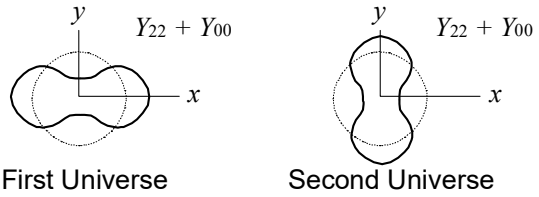


Contributions to average $a_{22}$ tend to cancel when adding universes

**Figure 9. Destructive Interference Adding Same Modes in Different Universes**

The variance (or, equivalently its square root, the standard deviation) of $a_{lm}$ ($l > 0$), however, is related to the squares of the $a_{lm}$ and thus must be a positive number, and not tend to zero. It would give us a measure of how great a contribution a particular spherical mode (given $l$ and $m$) makes to the physics of universes like ours. If we could somehow get an experimental value for that variance of $a_{lm}$ over an ensemble of universes, we would, as the saying goes, "be in business".

There actually is a trick that does something close to this, and we discuss it in Sect. 9.

### 9.2.3 A Trick to Get Many Measurements from Our One Universe

We don't have any extra universes we can access to make extra measurements of $a_{lm}$ in each, so what do we do?

If we consider that for given $l$, each $m$ is equally likely, then measuring those $m$ modes effectively gives us what we would get from extra measurements, for the same $l$, in different universes. If we average $a_{lm}$ ($l > 0$) over all $m$ for a given $l$, we will tend to get zero, just as we noted above for an average over different universes. So, the mean value for $a_{lm}$ ($l > 0$) over all $m$ isn't of much use to us.

However, if we average the square of the magnitude of $a_{lm}$ over all $m$ for a given $l$ we will get a non-zero value, a value that represents how much of that $l$ harmonic we have in the CMBR. This is for our universe, as observed, but that average can be a surrogate for an average for the same $l$ over different universes. Since $-l \le m \le l$, we have $2l + 1$ values of $m$ to use. For fairly large $l$, this essentially means good statistical values approaching the true values (over many universes) to high confidence.

Thus, we want to compute, for each $l$ value, the variance, which is labeled $C_l$, as

$$\boxed{\overline{|a_{lm}|^2} = \left\langle |a_{lm}|^2 \right\rangle = \left\langle a_{lm}^* a_{lm} \right\rangle = \frac{1}{2l+1} \sum_{m=-l}^{+l} a_{lm}^* a_{lm} = C_l \qquad \text{no sum on } l} \tag{9}$$

where the average symbol $\langle\ \rangle$ is considered to be for all $m$ values (given a single $l$ value) in our universe now.

An aside

Be aware that in the literature, $C_l$ is sometimes taken as the average over all $m$ values as above, and sometimes as just the value for a single $m$ averaged over many universes, as below.

$$\text{Sometimes one sees} \quad \left\langle a_{l'm'}^* a_{lm} \right\rangle = a_{l'm'}^* a_{lm}\, \delta_{l'l} \delta_{m'm} = C_l \qquad \left(\text{average over many universes}\right) \tag{10}$$

where the average symbol $\langle\ \rangle$ is considered to be for a single $m$ value (and single $l$ value) over many universes.

The connection between the two versions lies in the presumption that (10) for given $l$, over a large number of universes, would be the same for any $m$ (each $m$ mode would tend to have the same power). Thus, the average over all $m$, for given $l$, as in (9), would tend to equal (10). (10) is theoretical (we can never measure other universes), but (9) is something we can measure experimentally with the CMB data. We can, in fact, get $2l + 1$ separate measurements, implying, for large $l$, considerable confidence the computed value (9) is an accurate reflection of what is really going on (and not a statistical aberration.)

End of aside

Since power of any wave is proportional to the square of the amplitude of that wave, the variance can be thought of as a measurement of the power of the $l$ mode (including all $m$ values for that $l$ for (9)). Plotting $C_l$ vs $l$ is called a power spectral analysis. (See Appendix B for an intro to [review of] the theory of power spectral analysis.) Subject to further considerations to be discussed below, for the CMB, this gives us the power spectral analysis of Fig. 1 that has become so famous.

Note, in passing, that a system displaying the same statistics over many measurements in time or space as it does over many measurements from different similar systems in an ensemble is called ergodic. Here we are averaging over different measurements in space (spherical coordinate space) with the presumption that doing so gives us the same statistical results as measuring over different universes. So, our system is an ergodic one.

### 9.2.4 The Key Relationship

Note that if we use (4) with $f(\theta,\phi) = T(\theta,\phi)$ in (9), we get

$$\begin{aligned} C_l &= \left\langle |a_{lm}|^2 \right\rangle = \left\langle a_{lm}^* a_{lm} \right\rangle = \frac{1}{2l+1} \sum_{m=-l}^{+l} a_{lm}^* a_{lm} \qquad \text{no sum on } l \\ &= \frac{1}{2l+1} \sum_{m=-l}^{+l} \left( \int_0^{2\pi} \int_0^{\pi} Y_{lm}(\theta',\phi') T(\theta',\phi') \sin\theta' \, d\theta' \, d\phi' \right) \left( \int_0^{2\pi} \int_0^{\pi} Y_{lm}^*(\theta,\phi) T(\theta,\phi) \sin\theta \, d\theta \, d\phi \right) \\ &= \frac{1}{2l+1} \underbrace{\int_0^{2\pi} \int_0^{\pi}}_{\int_\Omega} \underbrace{\int_0^{2\pi} \int_0^{\pi}}_{\int_{\Omega'}} \left( \sum_{m=-l}^{+l} Y_{lm}(\theta',\phi') Y_{lm}^*(\theta,\phi) \right) T(\theta',\phi') T(\theta,\phi) \underbrace{\sin\theta' d\theta' d\phi'}_{d\Omega'} \underbrace{\sin\theta d\theta d\phi}_{d\Omega}. \end{aligned} \tag{11}$$

To streamline notation, we can use unit vector notation, where $\mathbf{n}$ is the unit vector pointing in the $\theta, \phi$ direction and $\mathbf{n}'$ is the unit vector pointing in the $\theta', \phi'$ direction. Thus, (11) is re-written as

$$\boxed{\begin{aligned} C_l &= \frac{1}{2l+1} \int_\Omega \int_{\Omega'} \left( \sum_{m=-l}^{+l} Y_{lm}(\theta',\phi') Y_{lm}^*(\theta,\phi) \right) T(\theta',\phi') T(\theta,\phi) \, d\Omega' d\Omega \\ &= \frac{1}{2l+1} \int_\Omega \int_{\Omega'} \left( \sum_{m=-l}^{+l} Y_{lm}(\mathbf{n}') Y_{lm}^*(\mathbf{n}) \right) T(\mathbf{n}') T(\mathbf{n}) \, d\Omega' d\Omega. \end{aligned}} \tag{12}$$

### 9.2.5 Finding $C_l$ Experimentally

We have a data set of discrete points of the CMB where each point has a $T$ value and an associated $\theta$, $\phi$ (or equivalently an $\mathbf{n}$). That is, we have $T(\theta,\phi) = T(\mathbf{n})$ in digital format. We can process this data via computer in either of two equivalent ways. The second is simpler and is preferred.

First way

Step 1. Use $f(\theta,\phi) = T(\theta,\phi) = T(\mathbf{n})$ in (4) to determine $a_{lm}$.

Step 2. Use $a_{lm}$ in (9).

Second way

An equivalent, and one step way, is simply to use (12) (which is simplified below in (14)).

### 9.2.6 Things to Know about $C_l$

Nomenclature and Units

$C_l$ is the variance of the spherical harmonic amplitudes $a_{lm}$ for fixed $l$. It is also known as the $l$ component of the power spectrum of the CMB (square of wave amplitude is proportional to power in a wave). Further, in its dependence on $l$, it is known as a correlation function, for reasons discussed below.

If $f(\theta,\phi) = T(\theta,\phi)$ in (4) and the spherical harmonics $Y_{lm}$ are unitless (which they are), then the $a_{lm}$ have units of temperature. Hence, $C_l$, via (9), has units of (temp)$^2$.

$C_l$ as a Correlation Function

Consider (12), where for two different locations on the sphere of the CMB (directions we see in space) $\mathbf{n}'$ and $\mathbf{n}$, the values of $T$ are particularly high, i.e., local maxima. There exists a certain $Y_{lm}$ at a given $l$ which also has peaks (local maxima) at these locations. Thus, in the integral of (12) this particular contribution, from the $T$ values at the two points, and the $Y_{lm}$ values at those points, will make a larger contribution to the value of $C_l$ than if the same pair of points did not display local maxima.

Thus, we will get larger values of $C_l$ for a given $l$ if there are peaks in the sky correlated with the peaks we find in $Y_{lm}$ for that $l$. Thus, we say $C_l$ represents a correlation between points a certain distance apart in the CMB. Actually, it is a measure of the correlation between all points integrated over the whole sphere for given $l$. The more such points peak at the between peaks distance of the $l$ spherical harmonic, the greater $C_l$. Thus, as a function of $l$, $C_l$ is a correlation function.

Independence of $C_l$ from Choice of Coordinate Reference Frame

One might question, from (12), if we would get different $C_l$ for different choices for our coordinate axes. (See Fig. A-2, pg. 29). For example, for a different alignment of our $z$ axis, the values for $\theta$ and $\phi$ would change for the two different points we integrate over, so one might expect the total integral to be different. However, the $C_l$ actually are independent of choice of coordinate axes, as shown below.

Showing $C_l$ independence from coordinate axes chosen

We will need something called the addition theorem for spherical harmonics, stated without proof below in (13). Note that $P_l$ is the Legendre polynomial of order $l$. (See Appendix A Sect. 15.1, pg. 27.)

$$P_l\underbrace{\left(\mathbf{n}'\cdot\mathbf{n}\right)}_{\cos\theta_{\mathbf{n}'\mathbf{n}}} = \frac{4\pi}{2l+1}\sum_{m=-l}^{+l} Y_{lm}\left(\theta',\phi'\right)Y_{lm}^{*}\left(\theta,\phi\right) = \frac{4\pi}{2l+1}\sum_{m=-l}^{+l} Y_{lm}\left(\mathbf{n}'\right)Y_{lm}^{*}\left(\mathbf{n}\right) \tag{13}$$

$\theta_{\mathbf{n}'\mathbf{n}}$ is the angle between $\mathbf{n}'$ (aligned with $\theta'$, $\phi'$) and $\mathbf{n}$ (aligned with $\theta$, $\phi$). Using (13) in (12), we have

$$\boxed{C_l = \frac{1}{4\pi}\int_{\Omega}\int_{\Omega'} P_l\left(\mathbf{n}'\cdot\mathbf{n}\right)T\left(\mathbf{n}'\right)T\left(\mathbf{n}\right)d\Omega' d\Omega}\,. \tag{14}$$

Relation (14) only depends on the angle between two points in the sky and the temperature at each of those points. Hence, it is independent of the particular coordinate axes alignment chosen.

Also, (14) seems simpler to evaluate than (12), so my guess (not being a practitioner in the field) would be that it is the preferred way to analyze the data. That is, use (14) instead of (12) in Sect. 9.2.5.

An Example: The Dipole ($l = 1$)

One can best understand the following example by first becoming familiar with Appendix A, Sect. 15.6.5 pg. 37. Fig. A-4 there shows one of the simplest spherical harmonics, the one for $l = 1$, i.e., the dipole. In the figure, three different dipole alignments along with their particular spherical harmonic coefficients $a_{lm}$ (for different $m$) are shown in the same coordinate system. However, an equivalent way to look at the figure is to consider the dipole fixed relative to the sky, but with different coordinate systems in each case. The $a_{lm}$ for each coordinate system (for the same dipole) are different (and are shown in the referenced section). However, in the sum of (9) over $m$, we should get the same $C_l$ in each case. The respective $|a_{lm}|^2$ contributions for each coordinate system in Fig. A-4 are shown summed together in the following chart.

**Comparison Chart for Fig. A-4, pg. 38**

($l = 1 \rightarrow 1/(2l + 1) = 1/3$ in (9))

| Fig. A-4 a) | Fig. A-4 b) | Fig. A-4 c) |
|---|---|---|
| $\frac{1}{3}\left(\lvert a_{1-1}\rvert^2 + \lvert a_{10}\rvert^2 + \lvert a_{11}\rvert^2\right) = C_l$ | $\frac{1}{3}\left(\lvert a_{1-1}\rvert^2 + \lvert a_{10}\rvert^2 + \lvert a_{11}\rvert^2\right) = C_l$ | $\frac{1}{3}\left(\lvert a_{1-1}\rvert^2 + \lvert a_{10}\rvert^2 + \lvert a_{11}\rvert^2\right) = C_l$ |
| $\frac{1}{3}\left( 0 + \frac{2X^2}{3} + 0 \right) = \frac{2X^2}{9}$ | $\frac{1}{3}\left( \frac{X^2}{3} + 0 + \frac{X^2}{3} \right) = \frac{2X^2}{9}$ | $\frac{1}{3}\left( \frac{2X^2}{6} + \frac{X^2}{6} + \frac{X^2}{6} \right) = \frac{2}{9}X^2$ |

**The conclusion**: The $C_l$ for the same pattern in the sky is the same as found in any coordinate system orientation.

Local Variation Implications for $C_l$ as a Correlation Function

We could consider either (12) or (14) and what happens for local maxima or minima temperature variations, though for simplicity, we will focus on (14). Fig. 10 depicts two local maxima schematically, projecting 3D to 2D for simplicity.

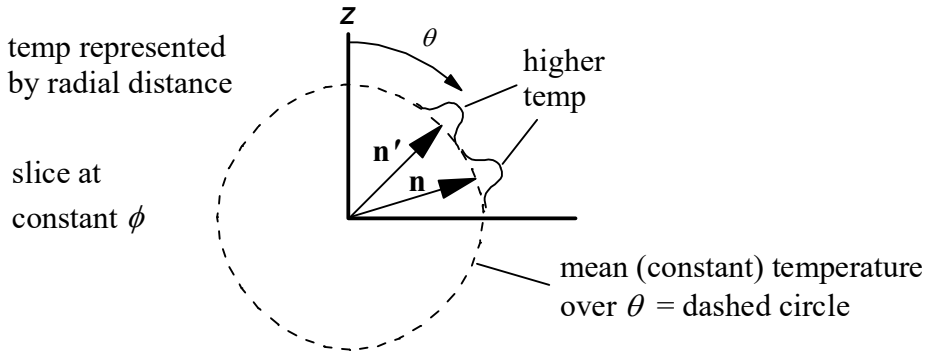


**Figure 10. Two (Hypothetical) Local Maxima in CMB**

In Fig. 10, we have two local solid angle regions where the temperature is higher than surrounding regions. That is, over a region of the integration of (14) (or (12)

$$T(\mathbf{n}')\Delta\Omega' \quad \text{and} \quad T(\mathbf{n})\Delta\Omega \qquad \text{both large for } \mathbf{n} \text{ and } \mathbf{n}' \text{ aligned as shown in Fig. 10.} \tag{15}$$

There is some Legendre polynomial $P_{l'}$, for some $l'$, that peaks regularly at the angular distance between $\mathbf{n}$ and $\mathbf{n}'$. Thus, in the region of higher temperatures, we would get a greater contribution to the integral (14) from $P_{l'}$ than from other $P_l$.

$$P_{l'}(\mathbf{n}'\cdot\mathbf{n})T(\mathbf{n}')T(\mathbf{n})\Delta\Omega'\Delta\Omega \qquad \text{high for regions where } \mathbf{n} \text{ and } \mathbf{n}' \text{ at temp peaks and } P_l \text{ peaks.} \tag{16}$$

For other regions, $P_{l'}$ may or may not peak, but the variation in $T$ does not, so the other regions would not contribute so much to the integral (14) for $l = l'$.

$$P_{l'}(\mathbf{n}'\cdot\mathbf{n})T(\mathbf{n}')T(\mathbf{n})\Delta\Omega'\Delta\Omega \qquad \text{low for regions where } \mathbf{n} \text{ and } \mathbf{n}' \text{ not at temp peaks and } P_l \text{ peaks} \tag{17}$$

For other $l$, and thus other $P_l$, the peaks in the $P_l$ would not correspond to the peak temperature regions in Fig. 10, so we would not get as great a contribution.

$$P_l(\mathbf{n}'\cdot\mathbf{n})T(\mathbf{n}')T(\mathbf{n})\Delta\Omega'\Delta\Omega \quad \text{low for } l \neq l' \text{ even in regions where } \mathbf{n} \text{ and } \mathbf{n}' \text{ at temp peaks and } P_l \text{ not at peaks} \qquad (18)$$

Note also that for $l'$, if there were more regions of local maxima in other parts of the sky separated by the same angle as for those maxima in Fig. 10, we would have more contributions like that of (16) to (14) and a higher value for $C_{l'}$.

**Bottom line**: For given $l$, $C_l$ is greater if there are more local extrema in the sky with angular separation similar to that displayed by the extrema in $P_l$. Thus, $C_l$ provides a measure of the correlation between number and level of variations in CMB temperature the sky for a particular value of $l$.

Since $l$ is inversely related to angular separation (angle = $180^o/l$), $C_l$ also represents a correlation between local extrema and their prevalence at a given angular separation.

The Variance of the Variance $C_l$

Note that $C_l$ is measured only for our universe, so it will have some error in it even for large, but finite, $l$ (where we have many $m$ to sample and sum over in (9) or (12)). Of course, we expect the error to be less, the larger the $l$, since there are more samples taken (more $m$). But there is some error nonetheless. If we had a nearly infinite number of universes in an ensemble, we could make a nearly infinite number of measurements, and pin $C_l$ down precisely. We are limited, instead, to our $2l + 1$ measurements for given $l$ in the one universe we do have.

We express our unknown error in $C_l$ as a confidence level, based on the usual relation for experimental standard deviation (19). (It is also common to use $N - 1$ in the denominator of (19), but cosmologists seem to use $N$.)

$$\text{Standard Deviation of } x = \sigma_x = \sqrt{\frac{\sum_{i=1}^{N}(x_i - \bar{x})^2}{N}} \qquad N \text{ measurements .} \qquad (19)$$

For us, $\bar{x} = C_l$, our average over all $m$ values ($2l + 1$ in number), as in (9). We have $N = 2l + 1$ measurements. So (19) becomes

$$\underbrace{\text{Standard Deviation of } |a_{lm}|^2}_{\text{Define as } \Delta C_l} = \sqrt{\frac{\sum_{m=-l}^{+l}\left(|a_{lm}|^2 - C_l\right)^2}{2l+1}} \qquad \text{no sum on } l . \qquad (20)$$

So,

$$\frac{\Delta C_l}{C_l} = \sqrt{\frac{\sum_{m=-l}^{+l}\left(\frac{|a_{lm}|^2}{C_l} - 1\right)^2}{2l+1}} \qquad \text{no sum on } l \qquad (21)$$

For some reason I have not been able to uncover, cosmologists assume the summation in the numerator of (21) is approximately 2. Thus,

$$\frac{\Delta C_l}{C_l} \approx \sqrt{\frac{2}{2l+1}} \quad \text{Cosmic variance} \quad (\text{no sum on } l) \quad \rightarrow \quad \text{standard deviation } \Delta C_l \approx \sqrt{\frac{2}{2l+1}}\, C_l . \qquad (22)$$

Strangely, though the LHS of (22) represents a standard deviation (divided by $C_l$), it is called the cosmic variance (one more source for confusion on this issue, as variance is typically the square of the standard deviation). For one standard deviation at given $l$ (= $\Delta C_l$), our confidence level is 68%; for two, 95%. These are the error bars one sees in a typical plot of the $C_l$ vs $l$. Note they are much wider for low $l$, than for higher values.

Keep in mind the difference between the "variance of the $a_{lm}$", which is $C_l$, and the "cosmic variance" $\Delta C_l$ which is the standard deviation of $C_l$ (divided by $C_l$). $\Delta C_l$ is a "variance" (not really) of a variance ($C_l$).

# 10 Theory: Converting Between Cartesian Fourier and Spherical Harmonics Analyses

## 10.1 Express $a_{lm}$ in Terms of Fourier Amplitude $A(\mathbf{k})$

As foreshadowed in Sect. 7.3, we will now express the spherical harmonic coefficients $a_{lm}$ for a given CMB temperature distribution in terms of the Fourier component coefficients for the same distribution. We do this for the general case where $a_{lm}$ can be at any radius $r$ from the origin, not just at the radius of the LSS.

We start by repeating (4) for any sphere of radius $r$, with some alternate notation employing the unit vector $\mathbf{n}$ from the origin to the unit radius sphere, and with the arbitrary function $f$ replaced with CMB temperature $T$.

$$a_{lm} = \int_0^{2\pi} \int_0^{\pi} Y_{lm}^*(\theta,\phi)\, \underbrace{T(\theta,\phi)}_{\text{at radius } r} \sin\theta\, d\theta\, d\phi = \int Y_{lm}^*(\mathbf{n})\, T(\mathbf{r})\, d\Omega \qquad \mathbf{r} = r\,\mathbf{n}. \tag{4}$$

Then, instead of the discrete form of $f(\mathbf{r}) = T(\mathbf{r})$ in (7), we use the continuous form shown in the lowest row of (7), repeated below, which describes the CMB temperature everywhere (not just on the spherical surface of the LLS).

$$T(\mathbf{r}) = \frac{1}{(2\pi)^3} \int A(\mathbf{k}) \overbrace{e^{ik_x x} e^{ik_y y} e^{ik_z z}}^{\text{Cartesian form}} d^3k = \frac{1}{(2\pi)^3} \int A(\mathbf{k})\, \overbrace{e^{i\mathbf{k}\cdot\mathbf{r}}}^{\text{general form}}\, d^3k \qquad \text{last row of} \tag{7}$$

Now use the Rayleigh plane wave expansion (6)

$$e^{i\mathbf{k}\cdot\mathbf{r}} = 4\pi \sum_{l'=0}^{\infty} \sum_{m'=-l'}^{l'} i^{l'} j_{l'}(kr) Y_{l'm'}^*(\theta_{\mathbf{k}},\phi_{\mathbf{k}}) Y_{l'm'}(\theta,\phi) = 4\pi \sum_{l'=0}^{\infty} \sum_{m'=-l'}^{l'} i^{l'} j_{l'}(kr) Y_{l'm'}^*(\mathbf{n}_{\mathbf{k}}) Y_{l'm'}(\mathbf{n}) \qquad \mathbf{k} = k\mathbf{n}_{\mathbf{k}} \tag{6}$$

to express (7) in terms of spherical harmonics/coordinates.

$$T(\mathbf{r}) = T(r\,\mathbf{n}) = \frac{1}{(2\pi)^3} \int A(\mathbf{k}) \left( 4\pi \sum_{l'=0}^{\infty} \sum_{m'=-l'}^{l'} i^{l'} j_{l'}(kr) Y_{l'm'}^*(\mathbf{n}_{\mathbf{k}}) Y_{l'm'}(\mathbf{n}) \right) d^3k\ . \tag{23}$$

Now put (23) into (4), where we use (81) of Appendix A in the second line,

$$\begin{aligned} a_{lm} &= \int Y_{lm}^*(\mathbf{n}) \left( \frac{1}{(2\pi)^3} \int A(\mathbf{k}) \left( 4\pi \sum_{l'=0}^{\infty} \sum_{m'=-l'}^{l'} i^{l'} j_{l'}(kr) Y_{l'm'}^*(\mathbf{n}_{\mathbf{k}}) Y_{l'm'}(\mathbf{n}) \right) d^3k \right) d\Omega \\ &= \frac{4\pi}{(2\pi)^3} \sum_{l'=0}^{\infty} \sum_{m'=-l'}^{l'} \left( \int A(\mathbf{k}) i^{l'} j_{l'}(kr) Y_{l'm'}^*(\mathbf{n}_{\mathbf{k}}) \underbrace{\left( \int \left( Y_{lm}^*(\mathbf{n}) Y_{l'm'}(\mathbf{n}) \right) d\Omega \right)}_{\delta_{ll'}\delta_{mm'}} d^3k \right) \\ &= \frac{4\pi}{(2\pi)^3} \int A(\mathbf{k}) i^{l} j_{l}(kr) Y_{lm}^*(\mathbf{n}_{\mathbf{k}})\, d^3k, \end{aligned} \tag{24}$$

where $a_{lm}$ here is at radius $r$ from the origin,
$A(\mathbf{k})$ is the Fourier coefficient for the $\mathbf{k}$ wave.

## 10.2 Express $C_l = \left\langle a_{l'm'}^* a_{lm} \right\rangle$ in Terms of Fourier Amplitudes $A(\mathbf{k})$

Now we express the variance $C_l$ in terms of $A(\mathbf{k})$ instead of $T(\mathbf{n})$ (as we did in (12) and (14)), and do so for any radius $r$.

First, we start with (9) or (10) (each uses a different way to take the mean), repeated below,

$$C_l = \left\langle |a_{lm}|^2 \right\rangle = \left\langle a_{l'm'}^* a_{lm} \right\rangle \qquad \text{no sum on } l \tag{9) or (10}$$

and insert the last row of (24) into it twice.

$$C_l = \left\langle a^*_{l'm'} a_{lm} \right\rangle = \left\langle \left( \frac{4\pi}{(2\pi)^3} \int A^*(\mathbf{k}')(-i)^{l'} j_{l'}(k'r) Y_{l'm'}(\mathbf{n}_{\mathbf{k}'}) d^3k' \right) \left( \frac{4\pi}{(2\pi)^3} \int A(\mathbf{k}) i^l j_l(kr) Y^*_{lm}(\mathbf{n}_{\mathbf{k}}) d^3k \right) \right\rangle$$

$$= \frac{(4\pi)^2}{(2\pi)^6} (-i)^{l'} i^l \left\langle \iint A^*(\mathbf{k}') A(\mathbf{k}) j_{l'}(k'r) j_l(kr) Y_{l'm'}(\mathbf{n}_{\mathbf{k}'}) Y^*_{lm}(\mathbf{n}_{\mathbf{k}}) d^3k' d^3k \right\rangle \tag{25}$$

$$= \frac{1}{4\pi^4} (-i)^{l'} i^l \iint \left\langle A^*(\mathbf{k}') A(\mathbf{k}) \right\rangle j_{l'}(k'r) j_l(kr) Y_{l'm'}(\mathbf{n}_{\mathbf{k}'}) Y^*_{lm}(\mathbf{n}_{\mathbf{k}}) d^3k' d^3k .$$

Second, we want to eliminate the primed quantities and simplify. To do this, we note in the last line of (25) that

$$\left\langle A^*(\mathbf{k}') A(\mathbf{k}) \right\rangle \;\rightarrow\; 0 \quad \text{for } \mathbf{k}' \neq \mathbf{k} , \tag{26}$$

since $A(\mathbf{k})$ can be positive or negative, and in sums over many universes (or many times or many $m$), its value and its negative will at times pair with the same $A^*(\mathbf{k}')$ and those two terms will cancel. Over large sums, enough pairings arise to give a total value approaching zero as the number of universes (number of times, number of $m$ values) approaches infinity.

However,

$$\left\langle A^*(\mathbf{k}') A(\mathbf{k}) \right\rangle \;\rightarrow\; (\text{some factor}) \left\langle |A(\mathbf{k})|^2 \right\rangle \neq 0 \quad \text{for } \mathbf{k}' = \mathbf{k} , \tag{27}$$

where $\left\langle |A(\mathbf{k})|^2 \right\rangle$ is a variance in $\mathbf{k}$ space, similar in some ways to $C_l$ in spherical harmonic space. This is some justification for the following, which is proven in Abramo and Pereira[1],

$$\left\langle A^*(\mathbf{k}') A(\mathbf{k}) \right\rangle = \left\langle |A(\mathbf{k})|^2 \right\rangle (2\pi)^3 \delta(\mathbf{k}' - \mathbf{k}) . \tag{28}$$

With (28), the last line of (25) turns into

$$C_l = \frac{2}{\pi} (-i)^{l'} i^l \int \left\langle |A(\mathbf{k})|^2 \right\rangle j_l(kr) j_{l'}(kr) Y_{l'm'}(\mathbf{n}_{\mathbf{k}}) Y^*_{lm}(\mathbf{n}_{\mathbf{k}}) \, d^3k \;\; . \tag{29}$$

Consider that things are isotropic in that waves varying in direction about the origin, but always having the same $|\mathbf{k}| = k$, will have the same $\left\langle |A(\mathbf{k})|^2 \right\rangle$. And our integral in (29) is effectively an integral in $\mathbf{k}$ space of a continuum of spherical surfaces, where sub-integration is carried out over each surface and then those surface integrals are integrated in the radial direction. For each of these spherical surfaces, we can take $\left\langle |A(\mathbf{k})|^2 \right\rangle = \left\langle |A(k)|^2 \right\rangle$ and use the same orthogonality relation in $\mathbf{k}$ space as we used in (24) in $\mathbf{r}$ space, to get

$$C_l = \frac{2}{\pi} (-i)^{l'} i^l \int \left\langle |A(k)|^2 \right\rangle j_l(kr) j_{l'}(kr) Y_{l'm'}(\mathbf{n}_{\mathbf{k}}) Y^*_{lm}(\mathbf{n}_{\mathbf{k}}) \underbrace{d^3k}_{k^2 d\Omega dk}$$

$$= \frac{2}{\pi} (-i)^{l'} i^l \int \left\langle |A(k)|^2 \right\rangle j_l(kr) j_{l'}(kr) \underbrace{\left( \int_\Omega Y_{l'm'}(\mathbf{n}_{\mathbf{k}}) Y^*_{lm}(\mathbf{n}_{\mathbf{k}}) d\Omega \right)}_{\delta_{ll'}\delta_{mm'}} k^2 dk \tag{30}$$

Or

$$C_l = \frac{2}{\pi} (-i)^l i^l \int \left\langle |A(k)|^2 \right\rangle j_l^2(kr) k^2 dk = \frac{2}{\pi} \underbrace{(-1)^l \left(i^2\right)^l}_{(-1)^{2l} = 1} \int \left\langle |A(k)|^2 \right\rangle j_l^2(kr) k^2 dk = \frac{2}{\pi} \int \left\langle |A(k)|^2 \right\rangle j_l^2(kr) k^2 dk . \tag{31}$$

and thus, (31) is the relationship we sought between $C_l$ and $A(\mathbf{k})$. Actually, it is a relationship between the variance in our spherical harmonic system and the variance in the Cartesian Fourier system. We will have more to say about this in Sect. 11.4

---

[1] Abramo, L. Raul, and Pereira, Thiago S., Testing gaussiantity, homogeneity and isotropy with the cosmic microwave background, *Advances in Astronomy*, Vol. 2010, Article ID 378203, 25 pages. http://arxiv.org/abs/1002.3173. See (12) and the line after (17).

# 11 Comparing Observation and Theory: Plotting $C_l$ vs $l$

## 11.1 Angular Variation

As shown in Appendix A, Sect. 15.6.7, pg. 39, the angular separation between variations, such as those shown in Fig. 10, for a given harmonic mode $l$, is

$$\text{angular variation} = \frac{180^o}{l} \qquad \left( = \frac{\pi}{l} \text{ in radians} \right) \tag{32}$$

## 11.2 Peaks in Power Spectrum

It turns out that the fundamental standing wave (see Fig. 3 pg. 4) of length $L$, via the mechanism depicted in Fig. 6, pg. 8, becomes a spherical harmonic with nodes separated by a little under 1°. In other words, the $C_l$ for the CMB (see Fig. 1, pg. 1) peaks at about $l = 200$ or so.

We will discuss the meaning of this and the other peaks later on.

## 11.3 Background in Power Spectral Analysis Needed for Subsequent Material

In Appendix B, pg. 39, we present a simplified, introductory overview of power spectra and how they are derived from the wave amplitude (and wave variance). This information will be needed as a prerequisite for the following section. Some readers may already know that material. Some may not, or may be a bit rusty on it.

## 11.4 Why CMB Plots Have $l(l+1)C_l/2\pi$ on the Vertical Axis Rather than $C_l$

The reason we see $l(l+1)C_l/2\pi$ on the vertical axis of typical CMB power spectrum plots such as Fig. 1, pg. 1, has to do with our conversion from Fourier analyses in Cartesian coordinates to spherical harmonic analysis in spherical coordinates (Sect.10.2, pg.19) plus our desire to work with spectral power (rather than variance) plots having log scaling on the $l$ axis.

The theory of inflation and subsequent expansion posit an effectively uniform (subject to subtleties) distribution of initial fluctuations in power across all wavelengths **k**, i.e., scale invariance. On average, no fluctuation wavelength has an intrinsic, enhanced power over any others. The dynamics of acoustic wave formation change this, of course, but initially, before that got started, the whole thing was egalitarian.

Representing this initially democratic situation is rather straightforward in Cartesian space, where each Fourier component of wave vector **k** would be independent of all others. But this becomes less straightforward for spherical harmonics where each different spherical harmonic amplitude $a_{lm}$ is a "funky" combination of the Fourier amplitudes $A(\mathbf{k})$, as shown in (24).

As we will see, this funkiness of spherical harmonics can be modified in an advantageous way by multiplying each $C_l$ by $l(l+1)/2\pi$. For the case of a universe with no acoustic wave formation, this should give us a curve in Fig. 1 of a straight horizontal line, subject to some subtleties beyond the scope of this discussion. So, any changes via acoustic wave formation seen in our universe would show up in the figure as deviations from the horizontal line and "jump out" at us. They would not be submerged in other, unrelated variations with $l$ due to the funkiness of spherical harmonics.

### 11.4.1 Relate $C_l$ to the Temperature Power Spectrum in $k$

From Appendix B, pg. 39, relation (117) the Fourier temperature power spectrum $P_T(k)$ is, with a conventional choice of constant to turn the proportional sign to an equal sign,

$$P_T(k) = \frac{k^2}{2\pi^2} \left\langle \left| A(k) \right|^2 \right\rangle . \tag{33}$$

As also shown in Appendix B, relation (118), with symbols changed to $k$ space below, shows how, given $P_T(k)$, we can determine the power over a given interval of a power spectrum,

$$\text{power between } k_1 \text{ and } k_2 = \int_{k_1}^{k_2} P_T(k)\, dk ,$$

where $P_T(k)$ is the power per unit $k$.

Solving (33) for $\left\langle \left| A(k) \right|^2 \right\rangle$ and inserting into (31) gives us

$$C_l = 4\pi \int P_T(k) j_l^2(kr)\, dk , \tag{34}$$

which relates the Fourier power spectrum $P_T(k)$, i.e., the power per unit $k$, in terms of $C_l$.

It is often desirable (and it is in CMB analysis) to work with the power per unit log $k$, instead of the power per unit $k$. If we plot such a quantity and have a log scale for $k$ on the horizontal axis, one can "eyeball" the power in an interval as simply the area one sees under the curve inside that interval.

To do this, we need to find an integrand for a relation parallel to (34) that is integrated with respect to $d(\log k)$. To find this integrand, reconfigure (34) as

$$C_l = 4\pi \int P_T(k) j_l^2(kr) k \underbrace{\frac{dk}{k}}_{d(\log k)} = 4\pi \int j_l^2(kr) \underbrace{k P_T(k)}_{\Delta_T^2(k)} d(\log k), \tag{35}$$

where we introduce the new symbol $\Delta_T^2(k)$. For this way of writing $C_l$, $\Delta_T^2(k) = k P_T(k)$ is power per unit log $k$.

### 11.4.2 Evaluate the Integral for $C_l$ with the Spherical Bessel Function in It

From integral tables, we find

$$\int j_l^2(z) d(\log z) = \frac{1}{2l(l+1)}. \tag{36}$$

From (36), therefore,

$$\begin{aligned} \frac{1}{2l(l+1)} &= \int j_l^2(kr) d(\log kr) = \int j_l^2(kr) \frac{d(kr)}{kr} = \int j_l^2(kr) \frac{rdk}{kr} \\ &= \int j_l^2(kr) \frac{d(k)}{k} = \int j_l^2(kr) d(\log k) = \frac{1}{2l(l+1)}. \end{aligned} \tag{37}$$

It is also known that a spherical Bessel function of order $l$ peaks when its argument is approximately given by $l$, i.e., $j_l^2(kr)$ peaks at about $kr = l$. Further, this peak is very narrow with $j_l$ effectively zero elsewhere. Hence, over the integral of (35), only a narrow range of $k$ contributes (around $k = l/r$), and over this range $\Delta_T^2(k)$ is approximately constant (and equal to $\Delta_T^2(k)(k = l/r)$.

Thus (35) becomes effectively

$$C_l \approx 4\pi \Delta_T^2(k = l/r) \underbrace{\int j_l^2(kr) d(\log k)}_{\substack{\text{only region near} \\ k=l/r \text{ contributes}}}. \tag{38}$$

With the last part of (37), we have

$$C_l \approx \frac{2\pi}{l(l+1)} \Delta_T^2(k = l/r). \tag{39}$$

### 11.4.3 Back to the Power Spectrum Plot

$\Delta_T^2(k)$ is the power spectrum per unit log $k$, for Fourier components in Cartesian coordinates. It is the number we really want to compare to our theory, which is grounded in Fourier analysis in Cartesian coordinates. So, a log plot (or any other plot) of $C_l$ (a spherical harmonics based number) vs $l$ distorts our perspective on what the real physics is doing (which we grasp more readily in Cartesian coordinate form).

Thus, if we multiply (39) by $l(l + 1)/2\pi$, we get (approximately) $\Delta_T^2(k)$, our Fourier analysis friend that we feel more at home with.

$$\frac{l(l+1)}{2\pi} C_l \approx \Delta_T^2(k = l/r) \qquad \text{the number typically plotted on CMB vertical axis vs } l. \tag{40}$$

## 11.5 Caveat on Wave Shape

To keep things simple and illustrate a point, we have depicted the acoustic wave shapes in Fig. 3, pg. 4, and elsewhere as sinusoidal components of the general random wave shape on the upper left portion of that figure, but that general shape is actually a bit more complicated. In fact, from both theory and analysis of the CMB, it is believed that via inflation, the large scale BAOs emerged, at least in large part, from primordial quantum harmonic oscillator fluctuations. Further, it appears the fundamental (lowest) state of those oscillators was, by far, the largest contributor to the fluctuations.

From elementary QM, we know (look it up if you don't recall) that the fundamental mode shape in space of a QM oscillator is Gaussian. See Fig. 11. The wave function $\psi$, and hence its probability density $|\psi|^2$, are normal (bell shape) curves in space. Thus, after inflation, the mass density variation would be expected to have similar shape.

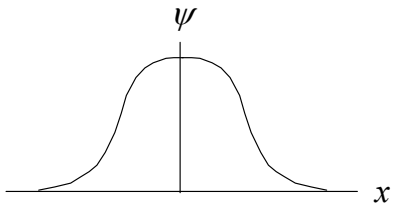


$$\psi = \sqrt{\frac{1}{\sigma\sqrt{2\pi}}}\, e^{-\frac{x^2}{4\sigma^2}} \quad \rightarrow \quad |\psi|^2 = \frac{1}{\sigma\sqrt{2\pi}}\, e^{-\frac{x^2}{2\sigma^2}}$$

**Figure 11. Gaussian Wave Form in Space for Ground State of Quantum Harmonic Oscillator**

The growth of pressure (sound) waves from density fluctuations described in Sect. 2.1 would then, via the appropriate dynamics, lead to sound waves (BAOs) of similar, Gaussian shape. The $n = 1$ wave of Fig. 3 is therefore a big component of a Gaussian shaped "lump". Similarly, the peaks and valleys between nodes of the other modes (such as $n = 2$ and 3 of Fig. 3) would comprise large components of shorter Gaussian shapes.

## 12 What the CMB Power Spectrum Tells Us

### 12.1 The First Peak

The first peak in Fig. 1, pg. 1, is at about $l \approx 200$ (a little less than 1°), which is related to the width $L$ of a fundamental mode. (See Fig. 3, pg. 4.) The length $L$ is the distance sound travels from just after the big bang to recombination. Cosmologists can calculate what that length should be. Knowing the distance to the LSS, they can then calculate what the angular separation (degrees, or equivalently the spherical mode number $l$) they would see. Note, from Fig. 12, that this angular measurement varies depending upon whether the universe is curved or not.

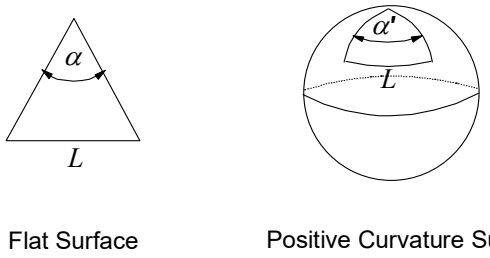


**Figure 12. Measuring Angles Seen to Ends of a Length *L***

A viewer looking at the ends of a known length at a given distance away in a positively curved space measures a larger angle between the ends than a viewer of the same length and given distance away in a flat space. In Fig. 12, $\alpha < \alpha'$. A negatively curved space would have a smaller angle than a flat space.

For the CMB data, the angular measurement of $L$, the width of our fundamental mode, shows up as the location of the first peak, i.e., the $l$ value, or equivalently the angle associated with that $l$ value via (32). If the calculated value of that angle ($l$ value) for a flat universe matches the CMB data location, we have a flat universe. If the measured angular value is larger (peak moves left, to lower $l$), we live in a positively curved universe; if smaller (peak moves right, to higher $l$), in a negatively curved one.

The data match for the peak location is, to fairly high accuracy, dead on for a flat universe.

Note that subtleties and uncertainties exist in the calculation and the measurement, and other parameters affect peak location to some degree as well, but higher peaks display the same dependence on curvature, so they can be used to check and refine the conclusions from the first peak. And for curvature, they check pretty well.

Those who have studied cosmology know this means the mass-energy density of the universe is what is known as the critical density $\rho_{cr}$, where a greater value means positive curvature, and a lesser one, negative curvature.

## 12.2 The Second Peak

Note that the second peak in Fig. 1 has *l* of about three times the fundamental peak, meaning its wavelength is 1/3 that of the $n = 1$ mode. This is what we expect theoretically, and this is what we observe. Note also that the valley between the two peaks has an *l* of about twice the $n = 1$ mode, meaning its wavelength is ½ that of the fundamental. Recall, we said the $n = 2$ mode had significant destructive interference and a mean compression/rarefaction of zero, so this makes sense, as well.

From Fig. 1, we can see that the second acoustic peak is much lower than the first. To understand this, we need first to recognize, from Fig. 3, pg. 4, and related discussion, that the odd numbered peaks (first, third, etc.) in the CMB power spectrum ($n = 1, 5, 9, \ldots$ in Fig. 3) are, overall, compressive in nature. Even number peaks (second, fourth, etc.) in the spectrum ($n = 3, 7, \ldots$ in Fig. 3) are, overall, rarefied in nature.

The oscillations result from massive baryons in more dense regions attracting more baryons with the resulting increase in baryons heating up the baryons and the photons they are in contact with. The photon pressure acts like spring to repel the baryons, so they spread and become less dense. After a time of expansion/rarefication the photon pressure decreases and gravity begins to pull baryons back closer together again. The whole process repeats leading to an oscillation that is analogous to a spring mass system. (See Fig. 13.) The mass in that system corresponds to baryon mass, the spring to photon pressure.

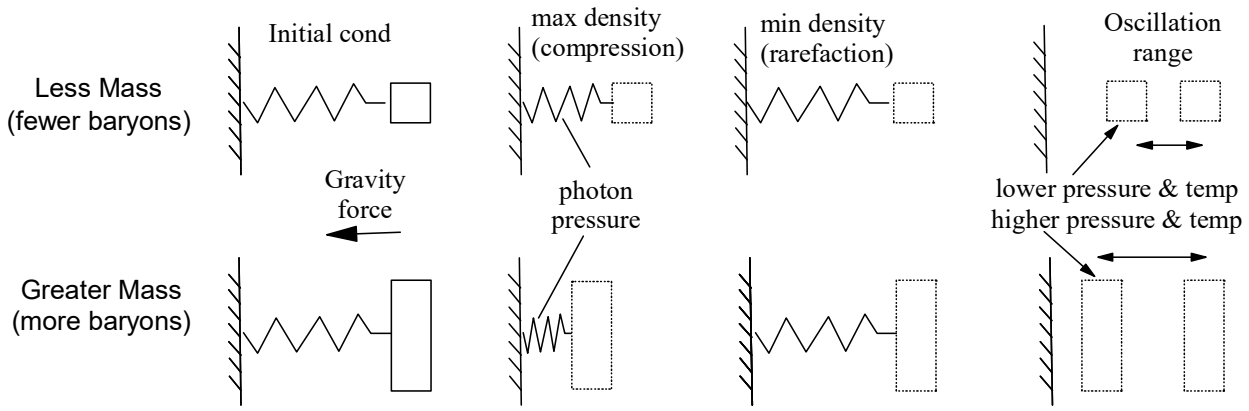


**Figure 13. Analogy of Spring Mass Oscillation to Baryon Acoustic Wave Oscillation**

Consider a given rarefied region, represented by the initial condition location in Fig. 13. With that same rarefied region, if there are more baryons in the adjacent denser region, the attraction will be greater, resulting in greater compression. A spring-mass system, like our BOAs, rebounds back to its initial condition (rarefied for BAOs) regardless of the extension (compressed for BAOs). But the extension (compression) is greater for greater mass.

We know the odd numbered peaks represent overall compression; the even ones, overall rarefication. If we have greater mass (more baryons) the compression level will be greater, so the odd numbered peaks will be more pronounced (higher in our spectral density plot, as in Fig. 1). Thus, increasing baryon number in our universe will increase the height of the odd numbered peaks relative to the even numbered peaks. We see this effect in Fig. 1, where there is a general trend for peak height to reduce with increasing *l*. The first peak (compressive) is much higher than the second (rarefied), and the third peak is about as high as the second.

The bottom line: The relative heights of the odd and even numbered peaks reflect the baryon density. Cosmologists can, of course, quantify this to give us a precise value.

## 12.3 Higher Numbered Peaks and Parameter Determination

The heights, locations (*l* values), and shapes of the peaks in the CMB spectral density tell us a whole lot about the various parameters of our universe, such as curvature, baryon density, dark matter density, dark energy density, etc. In general, a given parameter can affect more than one peak. For example, curvature affects the location of all peaks.

Conversely, characteristics of a given peak can be affected by more than one parameter. For example, different baryon density means a different oscillation frequency (slower for more mass) for all standing waves. This will change the value (slightly, as it turns out) of *l* for each peak, including the first. So, what we said before about the first peak determining curvature has to be modified a bit. We also have to take into account the shift in *l* value due to baryon density. Again, cosmologists do this as part of the analysis of the CMB spectrum.

The above is an example of degeneracy in cosmological parameters, where we need additional information from other parts of the CMB spectrum to pin down a particular parameter.

### 12.4 Dark Matter

Consider Fig. 13 where only some of the mass is baryonic and the rest, dark matter. The photon pressure only acts on the baryons, as dark matter is (at least to high degree) immune to the electromagnetic force carried by the photons. So, as the photon pressure repels the baryonic matter and causes it to move outward, the dark matter continues being attracted inward via gravity. At some point, it should again be drawn outward by the increased gravitational force of the baryonic matter that has moved outward.

This, of course, results in different wave forms from what we would have if all matter were baryonic. And thus, we have different shapes to our CMBR power spectrum plot in the two different cases. So, even if we can't see all of the normal matter in the universe, we can, via the CMBR plot, determine exactly how much normal matter and how much dark matter exists.

### 12.5 Dark Energy

As noted earlier, after recombination, the universe continues to expand, so our fundamental length $L$ (the distance sound travels from the big bang up to recombination) expands. How much it expands depends on the matter part of the mass-energy density of the universe plus the dark energy part. If dark energy causes the universal expansion rate to accelerate, we will measure a different stretched length for what was originally $L$, than if no dark energy existed.

And so, although dark energy played little role in the creation of our spherical harmonic modes, it affects their evolution afterwards in ways we can analyze, predict, and compare with observation. Hence, the CMBR plot can also tell us how much dark energy there is in the universe.

### 12.6 Collisionless (Silk) Damping

Note in Fig. 1 that the curve is damped at high $l$, and the peaks are not sharp spikes, but more like spread out humps, as one finds in a dynamic response curve with damping. This is called Silk damping.

A major cause of Silk damping is the finite length of time taken for recombination. It did not happen instantly at 380,000 years, but took some time, some tens of thousands of years, to transpire. In other language, the LSS is not infinitesimal in thickness. So, the photons will scatter a few times during this transition period, rather than be released unscathed in one grand, fleeting moment to forever hold the patterns impressed on them at a single time by the BAOs. The acoustic wave patterns (prior to "freezing") vary over time, resulting in humps rather than sharp spikes in Fig. 1.

Additionally, the average distance a photon travels (mean free path) increases over the transition period as the primordial plasma becomes more and more transparent to light. Wavelengths of the BAO for a higher $l$ are shorter. If the photon mean fee path is larger than the wavelength of the BAO for a given $l$, then, it turns out, the scattering will tend to smooth out the temperature contrasts at that $l$ value, and thus any peaks at that $l$ will be dampened. So, at shorter BAO wavelengths (higher $l$) power spectrum values will drop dramatically. And that is what we see in Fig. 1.

Other factors such as the baryon density (higher means more scattering of photons) affect the degree of damping. So precise determination of the degree of damping helps in pinning down key parameters.

It turns out that these effects contribute about equally to the suppression of anisotropies at small scales and give rise to the characteristic exponential damping tail seen in the very small angular scale anisotropies.

### 12.7 Other Things to Note

Analysis shows that had the Big Bang been a singularity, with no inflation, the anisotropies would be far greater than 1 part in $10^5$. Thus, the CMBR strongly supports a Big Bang starting at the end of an inflationary period and not from a singularity.

As a photon leaves a higher density region, it is essentially climbing out of a gravitational well, and thus loses energy (the gravitational red shift, where frequency is lowered). This is called the Sachs-Wolfe effect and leads to CMBR photon frequencies observed that indicate lower temperatures than actually existed at recombination. Cosmologists take this into account in the calculations leading to Fig. 1.

### 12.8 Plotting Theory vs Observation

Note that cosmologists use computer programs (see Sect. 14) to generate model CMB spectra. One inputs various parameters (dark energy percentage, baryon density, etc.) and the program spits out a power spectrum. By varying the parameters one gets a fit to the data and pins down which parameters yield that fit. See Fig. 14 for a graphic of what the CMB spectrum would look like for various values of certain parameters.

From graphs such as those of Fig. 14, cosmologists have determined our universe is flat to high accuracy and has values for dark energy of about 68%, dark matter of about 27%, and ordinary (baryonic) matter of about 5%. The resulting model is called the concordance model, or the ΛCDM model (for lambda cold dark matter, where lambda represents dark energy in cosmological constant form).

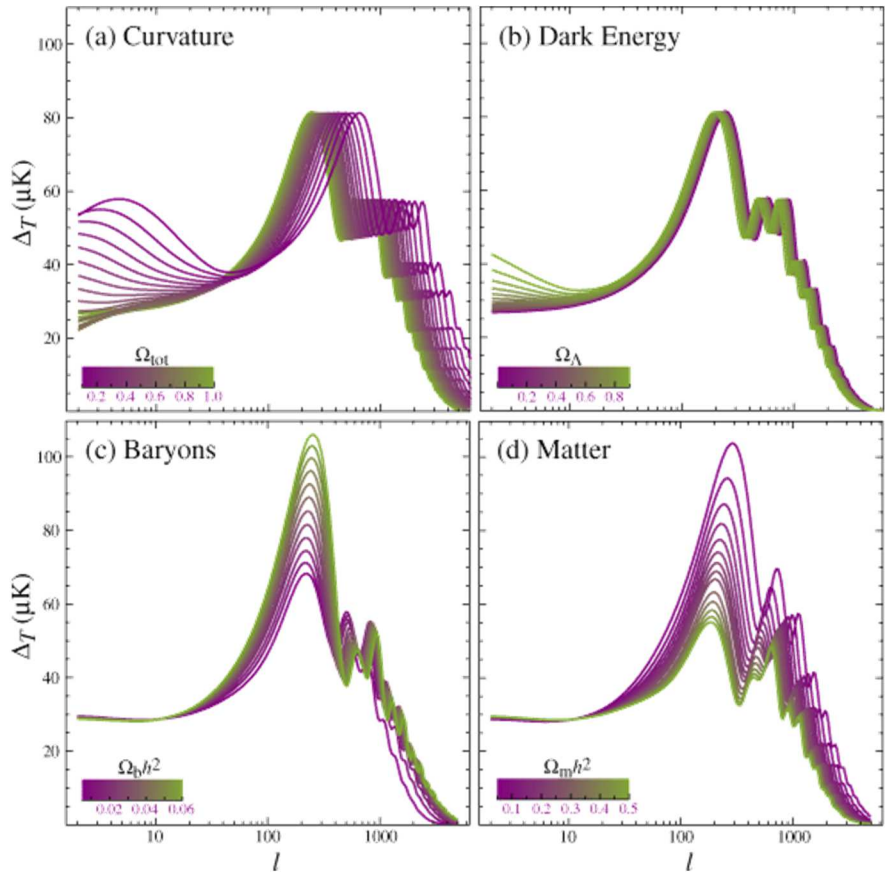


**Figure 14. Plots of the CMB Spectrum for Different Values of Key Parameters**

From webpage of Professors Hu and Dodelson http://background.uchicago.edu/~whu/araa/node15.html

### 12.9 Generate CMBR Curves Yourself for Different Universes

To generate CMB power spectral plots yourself, with different parameters (for dark energy, dark matter, baryon density, etc) go to NASA's https://lambda.gsfc.nasa.gov/bau/. Note that you change curvature in that plot by changing baryon matter, dark matter, and dark energy densities to sum to greater or less than 100% of the critical density.

## 13 Summary

We have explored the physical basis of baryonic acoustic oscillations in the early universe, and from that, developed the appropriate mathematics, at a relatively elementary level, that lead to the CMB power spectrum. We then showed, again at an elementary level, how that spectrum can be used to determine key cosmological parameters.

The presentation has been greater in depth than that of typical CMB popularization websites, yet markedly simpler and more rudimentary than that of typical cosmological textbooks. It has been intended to serve those with undergraduate, or better, backgrounds in physics, who are not (yet, or ever will be) specialists in the field.

## 14 Further Reading

Professor Whu at the University of Chicago does an excellent job of describing much of the material herein, with lots of graphics, on his website http://background.uchicago.edu/~whu/index.html. See also, Max Tegmark's page http://space.mit.edu/home/tegmark/cmb/pipeline.html. The math on those pages is not as extensive as that found herein.

For a next step, after this document, I recommend "Testing gaussianity, homogeneity and isotropy with the cosmic microwave background" by L. Raul Abarmo and Thiago S. Pereira (http://arxiv.org/abs/1002.3173). The math in that document is more advanced and more tersely presented than that herein.

Textbooks on the subject include *Modern Cosmology* by Scott Dodelson (Academic Press, 2003), *Physical Foundations of Cosmology* by Viatcheslav Mukhanov (Cambridge 2005), *The Cosmic Microwave Background* by Ruth Durrer (Cambridge, 2008) *Primordial Cosmology* by Patrick Peter and Jean-Philippe Uzan (Oxford, 2009). These books are quite advanced compared to the present document and represent entire graduate courses on the CMB. The present document is a good preliminary introduction to those texts.

# 15 Appendix A. Summary of Spherical Harmonics

A good reference for this material is Cahill[2]. What follows is only a summary and useful primarily for those who have studied this before, but are a little rusty.

To get to spherical harmonics, we have to start with Legendre polynomials.

## 15.1 Legendre Polynomials

Introduction

We start by noting that any function $f(x)$ can be expressed as a Taylor power series expansion,

$$f(x)=\sum_{s=0}^{\infty}c_s x^s \qquad c_s=\frac{f^{(s)}(0)}{s!} \qquad f^{(s)} \text{ is } s^{th} \text{ derivative of } f\,. \tag{41}$$

Legendre polynomials are of similar form,

$$P_n(x)=a_0+a_1x+a_2x^2+....+a_nx^n=\sum_{i=0}^{n}a_i x^i\,, \tag{42}$$

but are cut off after $n$ terms and have the following normalization (which may seem strange at first but helps in the long run)

$$P_n(x=1)=1 \qquad \rightarrow \qquad P_n(1)=a_0+a_1+a_2+....+a_n=1\,, \tag{43}$$

and orthogonality condition (note the interval of integration $-1 < x < 1$, which again is chosen because it eventually helps),

$$\int_{-1}^{1}P_n(x)x^m dx=0 \qquad m<n\,. \tag{44}$$

(44) says that each Legendre polynomial of order $n$ is orthogonal (over the interval shown) to any monomial $x^m$, provided $m < n$.

Thus, the first few Legendre polynomials (you can check if they meet the criteria of (43) and (44)) are

$$\begin{aligned} P_0(x)&=1 & P_3(x)&=\frac{1}{2}(5x^3-3x)\\ P_1(x)&=x & P_4(x)&=\frac{1}{8}(35x^4-30x^2+3)\\ P_2(x)&=\frac{1}{2}(3x^2-1) & P_5(x)&=\frac{1}{8}(63x^5-70x^3+15x). \end{aligned} \tag{45}$$

In a plot, they look like Fig. A-1.

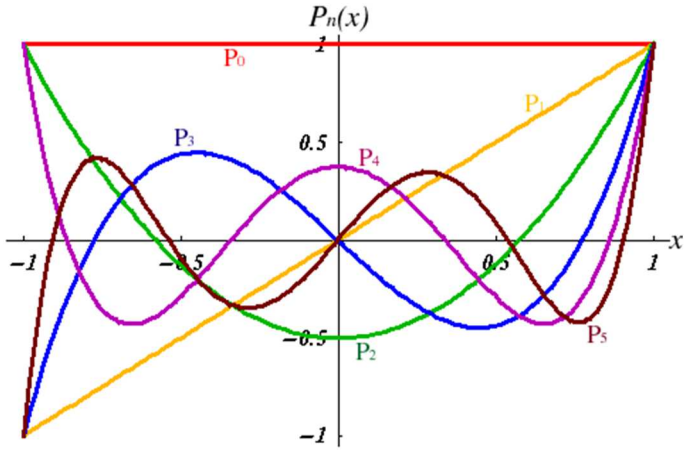


**Figure A-1. Plots of the First Six Legendre Polynomials**

There are shortcuts to finding Legendre polynomials called the Rodrigues formula ((8.8) pg. 306 of Cahill) and a recurrence relation ((8.38) of Cahill). The Rodrigues formula is

[2] Cahill, Kevin, *Physical Mathematics*, (Cambridge) 2013, pgs. 305-424.

$$P_n(x) = \frac{1}{2^n n!}\frac{d^n\left(x^2-1\right)^n}{dx^n}, \tag{46}$$

which you can check to see gives the first few polynomials in (45).

Helpful Way to Express Legendre Polynomials

It turns out to help in many things in physics (as we will see shortly for one example), if we take the argument $x$ for Legendre polynomials to be $\cos\theta$. That is, in (45) and (46),

$$\text{Take } x \to \cos\theta$$

$$\begin{aligned} P_0(\cos\theta) &= 1 & P_3(\cos\theta) &= \frac{1}{2}\left(5\cos^3\theta - 3\right) \\ P_1(\cos\theta) &= \cos\theta & P_4(\cos\theta) &= \frac{1}{8}\left(35\cos^4\theta - 30\cos^2\theta + 3\right) \\ P_2(\cos\theta) &= \frac{1}{2}\left(3\cos^2\theta - 1\right) & P_5(\cos\theta) &= \frac{1}{8}\left(63\cos^5\theta - 70\cos^3\theta + 15\cos\theta\right) \end{aligned} \tag{47}$$

$$P_n(\cos\theta) = \frac{1}{2^n n!}\frac{d^n\left(\cos^2\theta-1\right)^n}{d\left(\cos\theta\right)^n}. \tag{48}$$

With this substitution $x \to \cos\theta$, the horizontal axis in Fig. A-1 would go from $\theta = \pi$ ($x = -1$) to $\theta = 0$ ($x = 1$) with the vertical axis located at $\theta = \pi/2$ ($x = 0$). $P_1(\cos\theta)$ vs $\theta$ would then look like a half cycle of a cosine curve. Higher order Legendre polynomials would then be trigonometric functions of $\theta$ (though a bit more complicated that the ones we usually deal with.)

The integration limits of the orthogonality relations (44) were taken knowing in advance that we would be using the substitution $x \to \cos\theta$. The 1 to $-1$ integration range for $x$ corresponds to 0 to $\pi$ (which, since that is the range of variation of the $\theta$ coordinate in polar coordinates, we are foreshadowing where we might eventually use these relations). See Fig. A-2 below.

## 15.2 Legendre Polynomials Involved in Solutions to Key Physics Equations

Legendre polynomials help us in solving some key problems in physics, but we have a few more steps to go to see how.

### 15.2.1 Special Cases of a General Case Type Equation

General Case Type Equation

A general form of second order equation one runs into in physics is

$$\nabla^2 f + \left(g(\mathbf{x})\right) f = 0 \tag{49}$$

where $\nabla^2$ is the Laplacian and $g(\mathbf{x})$ is a general function of space. One example is the time independent Schrödinger equation with $f = \psi$,

$$-\frac{\hbar^2}{2\mu}\nabla^2\psi + V(\mathbf{x})\psi = E\psi \;\rightarrow\; \nabla^2\psi + \underbrace{\frac{2\mu}{\hbar^2}(E-V)}_{g(\mathbf{x})}\psi = 0. \tag{50}$$

Special Case, $g$ = constant

A special case of (49), where $g(\mathbf{x})$ is a constant (equal to $k^2$ below), is referred to as the Helmholtz equation,

$$\nabla^2 f + k^2 f = 0. \tag{51}$$

The solutions to the Helmholtz equation are spatial (static) waves. So, one should (rightfully) consider the spatial oscillations in the CMB could be described mathematically by the solutions to it. More on this later.

Note that (51) can be expressed in Cartesian or spherical coordinates (or any other coordinates, though we won't be concerned with those others). In Cartesian coordinates, (51) has solutions of form

$$f(x) \propto \sin kx,\ \cos kx, \text{ or } e^{ikx}\left(= \cos kx + i\sin kx\right) \quad \text{1D case}. \tag{52}$$

Relation to Wave Equation

Consider the wave equation

$$\nabla^2 f - \frac{1}{v^2}\ddot{f} = 0 \quad \xrightarrow{1D} \quad f'' - \frac{1}{v^2}\ddot{f} = 0\,, \tag{53}$$

where $v$ is the speed of the wave. This has solution

$$f = Ae^{i(\omega t - kx)} \quad \text{so} \quad \ddot{f} = -\omega^2 Ae^{i(\omega t - kx)} = -\omega^2 f,, \tag{54}$$

with which (53) becomes

$$f'' + \frac{\omega^2}{v^2} f = 0 \quad \text{with} \quad k^2 = \frac{\omega^2}{v^2} \;\rightarrow\; f'' + k^2 f = 0 \quad \xrightarrow{3D} \quad \nabla^2 f + k^2 f = 0, \tag{55}$$

and thus, the wave equation reduces to the Helmholtz equation (51). So, that equation is a key one in physics.

Special Case $g = 0$

For $g = 0$, we have the Laplace equation. For $f = \Phi$, the electric potential in a region free of charge, is a key relation for electrostatics. For Newtonian gravity, $f = \Phi$ would represent the gravitational field in a region free of mass.

$$\text{Laplace eq (e.g., electric potential in region of zero charge)} \qquad \nabla^2 \Phi = 0 \quad (\text{where } g = 0) \tag{56}$$

Special Case, Spherical Coordinates with $g = g(r)$

Cases where (49) has $g$ dependence only on the radial distance $r$ from the origin of the coordinate system used,

$$\nabla^2 f + g(r) f = 0\,, \tag{57}$$

are common. One example is the Schrödinger equation applied to the hydrogen atom, comprising an electron in the field of a proton's coulomb potential $V(r) = e^2/4\pi r$.

$$\text{Schroedinger eq, H atom} \qquad -\frac{\hbar^2}{2\mu}\nabla^2\psi + V(r)\psi = E\psi \;\rightarrow\; \nabla^2\psi + \underbrace{\frac{2\mu}{\hbar^2}(E - V)}_{g(r)}\psi = 0 \tag{58}$$

For problems of this type, spherical coordinates work best, and we express $\nabla^2$ in terms of $r$, $\theta$, and $\phi$.

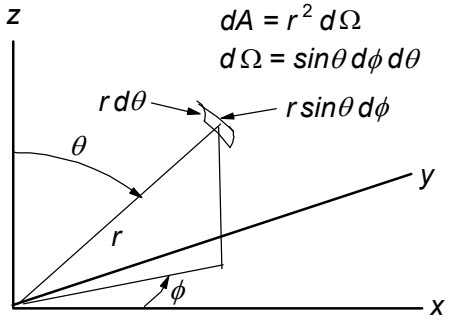


**Figure A-2. Spherical Coordinates with Differential Solid Angle $d\Omega$ Shown**

Special Case, Spherical Coordinates on 2D Surface of Sphere

If we wish to examine behavior of something on the surface of a sphere (such as the CMB radiation), we can fix $r$ in (57), and examine the resulting solution. That solution would have functional dependence only on $\theta$ and $\phi$. In effect, $g(r)$ = const in (57), and we would essentially be solving the Helmholtz equation (the equation for spatially varying static waves) on the surface of the sphere.

In this case, we should expect the behavior of $f$ with respect to $\theta$ and $\phi$ to parallel that of the solutions to the Schrödinger equation for the hydrogen atom. This should help most readers follow the remaining parts of this appendix, since most have some familiarity with that problem.

### 15.2.2 Solving the 2D Surface of a Sphere Case

Separation of Variables to Solve $g(r)$ Case

In cases where $g$ is a symmetric function of $r$ (purely a function of $r$ and not $\theta$ or $\phi$), then the problem of solving (49) simplifies. We try a separation of variables approach, i.e., we separate $f$ into functions dependent on $r$, $\theta$, and $\phi$, as follows.

$$f(r,\theta,\phi) = R(r)\underbrace{\Theta(\theta)\Phi(\phi)}_{Y(\theta,\phi)} = R(r)Y(\theta,\phi) \qquad \text{works for } g = \text{ only a function of } r \tag{59}$$

We then substitute (59) into (57), where $\nabla^2$ is expressed in spherical coordinates. When we do this (again, this is a summary review, we aren't going through all the steps), we find the following three separated equations, each only involving one coordinate.

$$\frac{1}{R}\frac{d}{dr}\left(r^2\frac{dR}{dr}\right) + g(r)r^2 = l(l+1) \qquad (l \text{ an integer. See why below.}) \qquad \underline{\text{Radial equation}} \tag{60}$$

$$\frac{d^2\Phi}{d\phi^2} + m^2\Phi = 0 \qquad \begin{pmatrix} m \text{ an integer and } -l \le m \le l. \text{ See why below.} \\ \text{This is actually Helmholtz eq with } x \to \phi. \end{pmatrix} \tag{61}$$

$$\frac{1}{\sin\theta}\frac{d}{d\theta}\left(\sin\theta\frac{d\Theta}{d\theta}\right) + \left(l(l+1) - \frac{m^2}{\sin^2\theta}\right)\Theta = 0 \qquad \underline{\text{associated Legendre equation}} \tag{62}$$

Using separation of variables we have converted a partial differential equation in three variables, which is generally very difficult to solve, into three separate ordinary differential equations, each in only a single function dependent on a single independent variable.

Radial Equation (not needed for CMBR analysis)

While we will ignore (60), as we are only dealing with functions on a spherical surface (at constant $r$), we note that it gives rise in QM to the radial part of the hydrogen atom wave function and in doing so, the fundamental energy eigenvalues.[3]

Φ Equation

The Helmholz equation in $\phi$, (61), is readily solved as

$$\Phi_m(\phi) = \frac{e^{im\phi}}{\sqrt{2\pi}} \qquad \text{One solution for each value of integer } m., \tag{63}$$

where the constant of the denominator is chosen so Φ is appropriately normalized (over $0 \le \phi \le 2\pi$). Note (63) expresses a (complex) wave oscillation as one progresses in the $\phi$ direction. We stated in (61) that $m$ must be an integer. The reason is that its solution (63) can only be single valued (as one progresses around $\phi$ past 360º), if $m$ is an integer. The number of nodes in 360º increases directly with $m$.

Associated Legendre Equation

There is a fair amount of algebra involved in determining $\Theta(\theta)$ of (62), the associated Legendre equation, but we cut to the chase here. For each different $l$ and each different $m$, there is a separate solution to (62), which we label as $\Theta_{lm}$. These solutions are proportional to entities called the associated Legendre polynomials, labeled as $P_{lm}$, which are closely related to Legendre polynomials. Thus, where we will later choose the proportionality constant to suit out needs, (62) can be re-written

[3] Note that for the special case $g(r) =$ constant (57) becomes the Helmholtz equation, and we have a different radial equation (60). For that constant equal to zero, $g(r) = 0$, (57) becomes the Laplace equation, with yet a different radial equation. However the angular dependent equations (61) and (62) are the same for $g(r)$ isotopic or constant (whether that constant is zero or not). Thus, in the discussion that follows regarding the solutions to (61) and (62), all conclusions are the same for the 3D spherical forms of each of the Helmholtz equation (51), the Laplace equation (56), the hydrogen atom Schrödinger equation (58), any case with isotropic $g(\mathbf{x})$ (57), and any case on the 2D surface of a sphere (like the CMB analysis). In the literature, one sometimes reads that the solution forms we are about to explore (associated Legendre polynomials, in particular) are derived from the Laplace equation, and sometimes from the Helmholtz equation or general isotropic form for $g$. Hopefully, this footnote will avoid confusion when you run into such statements.

for $\Theta_{lm} = (\text{constant})\, P_{lm}$ , as

$$\frac{1}{\sin\theta}\frac{d}{d\theta}\left(\sin\theta\frac{dP_{lm}}{d\theta}\right)+\left(l(l+1)-\frac{m^2}{\sin^2\theta}\right)P_{lm}=0 \quad \left(\frac{P_{lm}\text{ is }\underline{\text{associated Legendre polynomial}}}{\text{that solves associated Legendre equation}}\right). \tag{64}$$

If one goes through the math (see Cahill, we are only summarizing), one finds $P_{lm}$ in (64) to be (where we use the symbol "$l$" in place of "$n$" in the Legendre polynomial symbol)

$$\overbrace{P_{lm}}^{\substack{\text{associated}\\ \text{Legendre}\\ \text{polynomial}}} = \sin^m\theta\frac{d^m}{d\cos^m\theta}\underbrace{\overbrace{P_l\,(\cos\theta)}^{\substack{\text{Legendre}\\ \text{polynomial}}}}_{x\to\cos\theta} \qquad (l \text{ and } m \text{ integers with } -l\le m\le l\text{; no sum on } m). \tag{65}$$

The solutions to (64) are related to our earlier discussed Legendre polynomials via (65) where we take $x \to \cos\theta$, as discussed in Sect. 15.1. We note that it is common in the literature to write the argument of $P_{lm}$ as $\cos\theta$ instead of $\theta$. In that case, (65) becomes

$$P_{lm}(\cos\theta) = \left(1-\cos^2\theta\right)^{m/2}\frac{d^m}{d\cos^m\theta}P_l\,(\cos\theta) \qquad (l \text{ and } m \text{ integers with } -l\le m\le l). \tag{66}$$

You can check that the first few Legendre polynomials in (47), used in (66), actually solve (64).

Using Rodrigues formula (46) (with $x \to \cos\theta$) in (66), we get

$$\begin{aligned} P_{lm}(\cos\theta) &= \left(1-\cos^2\theta\right)^{m/2}\frac{d^m}{d\cos^m\theta}\frac{1}{2^l\,l!}\frac{d^l\left(\cos^2\theta-1\right)^l}{d(\cos\theta)} \\ &= \frac{1}{2^l\,l!}\left(1-\cos^2\theta\right)^{m/2}\frac{d^{m+l}\left(\cos^2\theta-1\right)^l}{d\cos^{m+l}\theta}. \end{aligned} \tag{67}$$

The bottom row of (67) only makes sense if $m+l\ge 0$ with $m + l$ an integer. Since $m$ is an integer (see above), then $l$ must be. Further, if $m$ exceeds $l$, then any derivative in that bottom row will yield zero for $P_{lm}$. Thus, we justify what was stated in (60), (61), (65), and (66) about $l$ and $m$.

When all is said and done, the first several associated Legendre polynomials, found via (67), look like

$$\begin{aligned} &P_{00}=1 \quad && P_{10}=\cos\theta && P_{20}=\frac{1}{2}\left(3\cos^2\theta-1\right) && P_{30}=\frac{1}{2}\cos\theta\left(5\cos^2\theta-3\right) \\ & && P_{11}=-\sin\theta && P_{21}=-3\sin\theta\cos\theta && P_{31}=-\frac{3}{2}\sin\theta\left(5\cos^2\theta-1\right) \\ & && && P_{22}=3\sin^2\theta && P_{32}=15\cos\theta\sin^2\theta \\ & && && && P_{33}=-15\sin^3\theta \end{aligned} \tag{68}$$

where $P_{l-m}=(-1)^m\frac{(l-m)!}{(l+m)!}P_{lm}$ .

To check, and strengthen one's understanding, any of (68) can be inserted into (64) to verify that they are indeed solutions to the associated Legendre equation.

## 15.3 Completeness and Orthonormality of $P_l^m$

### 15.3.1 Completeness

Other than arbitrary constants by which they could be multiplied, all possible solutions to the associated Legendre equation are included in $P_{lm}$ of (66), so the set of those solutions shown there spans the space of all possible solutions over $\theta$. This is similar to the 1D spatial (static) wave (Helmholtz) equation (51) where the set of all $e^{ik_n x}$ , where $k_n = n2\pi/L$ spans the space of all solutions to that equation over the interval treated.

Further, we know from the Fourier theorem that the solutions $e^{ik_n x}$ span the space of *all* possible functions of $x$ over the interval, not just functions that are specific solutions to the Helmholtz equation. Similarly, the associated Legendre polynomials $P_{lm}(\cos\theta)$ span the space of all possible functions of $\theta$, not simply those that are solutions to the associated Legendre equation.

Thus, the set $\underline{P_{lm}}\,(\cos\theta)$ is complete over $\theta$. Any possible function of $\theta$ can be shown equal to a sum of $a_{lm}\,\underline{P_{lm}}\,(\cos\theta)$ over all $l$ and $m$, where the constant coefficient $a_{l'm'}$ represents how much of $P_{l'm'}$ is present. For example, in the $m = 0$ case (no variation in the $\phi$ direction since $e^{im\phi} = 1$ for $m = 0$), any function purely of $\theta$ (and not $\phi$) can be represented as

$$f(\theta) = a_{00}P_{00}(\cos\theta) + a_{10}P_{10}(\cos\theta) + a_{20}P_{20}(\cos\theta) + \ldots = \sum_{l=0}^{\infty} a_{l0}P_{l0}(\cos\theta) \qquad m = 0\,. \tag{69}$$

### 15.3.2 Orthonormality

For same $m$

We first state, then shortly after that prove, the orthogonality of $\underline{P_{lm}}$ which have the same $m$, but different $l$. Note that since $\underline{P_{lm}}$ is real (see (68), for examples), we do not need to take the complex conjugate of $\underline{P_{lm}}$ times $\underline{P_{lm}}$, as is done, for example, with quantum wave functions.

$$\int_{-1}^{1} P_{l'm}(x)\,P_{lm}(x)\,dx = 0 \qquad l \neq l',\ \text{same } m,\ x = \cos\theta\,. \qquad \text{(no sum on } m\text{)} \tag{70}$$

The inner product of $\underline{P_{lm}}$ with itself (same $m$ and same $l$) represents the normalization and is (reference to proof given below)

$$\int_{-1}^{1} P_{l'm}(x)\,P_{lm}(x)\,dx = \frac{2}{2l+1}\frac{(l+m)!}{(l-m)!} \qquad \text{same } l,\ \text{same } m,\ x = \cos\theta\,. \quad \text{(no sum on } l,\ m\text{)} \tag{71}$$

We can combine (70) and (71), and substitute $\cos\theta$ for $x$, to yield the orthonormality condition for $\underline{P_{lm}}$

$$\begin{aligned}\int_{-1}^{1} P_{l'm}(x)\,P_{lm}(x)\,dx = \frac{2}{2l+1}\frac{(l+m)!}{(l-m)!}\delta_{ll'} \quad &= \int_{\pi}^{0} P_{l'm}(\cos\theta)\,P_{lm}(\cos\theta)\,d(\cos\theta) = -\int_{\pi}^{0} P_{l'm}(\cos\theta)\,P_{lm}(\cos\theta)\sin\theta\,d\theta \\ &= \int_{0}^{\pi} P_{l'm}(\cos\theta)\,P_{lm}(\cos\theta)\sin\theta\,d\theta = \frac{2}{2l+1}\frac{(l+m)!}{(l-m)!}\delta_{ll'}. \qquad \text{same } m\ (\text{no sum on } l,m)\end{aligned} \tag{72}$$

For different $m$

On pg. 319, Cahill derives the orthonormality relations for the $\underline{P_{lm}}$, for different $m$, but, as we will see, we will not need these.

Proof of (70)

To prove the orthogonality condition (70), we start by rearranging (64),

$$\frac{1}{\sin\theta}\frac{d}{d\theta}\left(\sin\theta\frac{dP_{lm}(\cos\theta)}{d\theta}\right) - \frac{m^2}{\sin^2\theta}P_{lm}(\cos\theta) = l(l+1)\,P_{lm}(\cos\theta) \qquad \begin{matrix}\text{associated Legendre}\\ \text{equation, rearranged.}\end{matrix} \tag{73}$$

If we consider $m$ fixed, then (73) can be considered an eigenvalue problem with eigenfunctions $\underline{P_{lm}}$ and eigenvalues $l(l + 1)$. Eigenfunctions are always orthogonal. Thus, for integration over the stated interval, we have (70).

Proof of (71)

If I have time, I may someday write out the proof of (71), which I never actually looked at myself before writing this. (I had simply accepted the result, like one accepts integral formulas in a table without working them through oneself.) For now I simply note that it is only algebra, comprising substitution of the last line of (67) with $\cos\theta \to x$ into the LHS of (71) and working it all out. The full proof can be found in Arfken and Weber[4]. Cahill merely states the result (72) without proof.

[4] Arfken, George B., and Weber, Hans J., *Mathematical Methods for Physicists* (Academic Press, San Diego) 1995, pgs. 726-727.

## 15.4 Completeness and Orthonormality of $Y_{lm}(\theta,\phi)$

### 15.4.1 Completeness

We have realized that $\underline{P_{lm}}$ is complete over $\theta$ for the interval 0 to $\pi$. Using similar logic as we had with the 1D Helmholtz equation (51) and its solutions being complete (spanning the space of all functions over $x$), the solutions $e^{im\phi}$ to equation (61) (identical in form to the Helmholtz equation) are complete over $\phi$ for the interval 0 to $2\pi$. Thus, from (59), where we now realize we need the $l$ and $m$ subscripts,

$$Y_{lm}(\theta,\phi)=\Theta_{lm}(\theta)\Phi_m(\phi)=(\text{constant})\,P_{lm}(\cos\theta)\frac{e^{im\phi}}{\sqrt{2\pi}} \qquad \text{no sum on } m \tag{74}$$

is complete over the 2D space defined by $0\le\theta\le\pi$ and $0\le\phi\le 2\pi$. Any function of $\theta$ and $\phi$ can be described by a sum over $l$ and $m$ of terms $a_{lm}\,Y_{lm}$, where the $a_{lm}$ are appropriate constants.

### 15.4.2 Orthonormality

Normalization

Using (74), integrating $\left|Y_{lm}(\theta,\phi)\right|^2$ over all $\theta$ and $\phi$ (effectively integrating over the surface of a sphere with radius $r = 1$ in Fig. A-2 pg. 29), and normalizing by setting the result equal to unity, we have

$$\begin{aligned}
1&=\oint Y_{lm}^*(\theta,\phi)Y_{lm}(\theta,\phi)\,d\Omega=\int_0^{2\pi}\int_0^{\pi}Y_{lm}^*(\theta,\phi)Y_{lm}(\theta,\phi)\sin\theta\,d\theta\,d\phi \qquad (\text{no sum on } l.m)\\
&=\int_0^{2\pi}\int_0^{\pi}\Theta_{lm}^*(\theta)\Phi_m^*(\phi)\Theta_{lm}(\theta)\Phi_m(\phi)\sin\theta\,d\theta\,d\phi\\
&=\int_0^{2\pi}\int_0^{\pi}\left|\text{constant}\right|^2 P_{lm}(\cos\theta)P_{lm}(\cos\theta)\frac{e^{-im\phi}}{\sqrt{2\pi}}\frac{e^{im\phi}}{\sqrt{2\pi}}\sin\theta\,d\theta\,d\phi \qquad (75)\\
&=\left|\text{constant}\right|^2\int_0^{\pi}P_{lm}(\cos\theta)P_{lm}(\cos\theta)\sin\theta\,d\theta\underbrace{\frac{1}{2\pi}\int_0^{2\pi}d\phi}_{=1}\\
&=\left|\text{constant}\right|^2\int_0^{\pi}P_{lm}(\cos\theta)P_{lm}(\cos\theta)\sin\theta\,d\theta.
\end{aligned}$$

From the last line of (72), with the last line of (75) equal to one, we see

$$\left|\text{constant}\right|^2=\frac{2l+1}{2}\frac{(l-m)!}{(l+m)!}. \tag{76}$$

Thus, from (74) we see the spherical harmonics are

$$\boxed{Y_{lm}(\theta,\phi)=\sqrt{\frac{2l+1}{2}\frac{(l-m)!}{(l+m)!}}\,P_{lm}(\cos\theta)\frac{e^{im\phi}}{\sqrt{2\pi}} \qquad \text{no sum on } l \text{ or } m.} \tag{77}$$

Our normalization constant is the quantity inside the square root sign above.

Orthogonality

For the same $m$ and $l' \ne l$

From (72), we see that for the same $m$ and any $l' \ne l$, $P_{l'm}$ and $\underline{P_{lm}}$ are orthogonal over $\theta$. Thus, $Y_{l'm}$ and $Y_{lm}$ must also be orthogonal over an entire sphere, i.e.,

$$\int_0^{2\pi}\int_0^{\pi} Y_{l'm}^*(\theta,\phi)\,Y_{lm}(\theta,\phi)\sin\theta\,d\theta\,d\phi \qquad (\text{no sum on } m,\ l'\neq l)$$
$$=\int_0^{2\pi}\int_0^{\pi}\frac{2l+1}{2}\frac{(l-m)!}{(l+m)!}P_{l'm}(\cos\theta)\,P_{lm}(\cos\theta)\frac{e^{-im\phi}}{\sqrt{2\pi}}\frac{e^{im\phi}}{\sqrt{2\pi}}\sin\theta\,d\theta\,d\phi \tag{78}$$
$$=\frac{2l+1}{2}\frac{(l-m)!}{(l+m)!}\underbrace{\int_0^{\pi}P_{l'm}(\cos\theta)\,P_{lm}(\cos\theta)\sin\theta\,d\theta}_{=0\text{ for }l'\neq l}=0\ .$$

(78) tells us that for the same $m$ and $l'\neq l$, the spherical harmonics are orthogonal.

For different $m'$ and $m$ and any $l$ and $l'$

For different $m'$ and $m$, regardless of $l'$ and $l$, we have

$$\int_0^{2\pi}\int_0^{\pi} Y_{l'm'}^*(\theta,\phi)\,Y_{lm}(\theta,\phi)\sin\theta\,d\theta\,d\phi \qquad (m'\neq m,\ l' \text{ and } l \text{ may be same or different, no sum on } l,m)$$
$$=\int_0^{2\pi}\int_0^{\pi}\sqrt{\frac{2l'+1}{2}\frac{(l'-m')!}{(l'+m')!}}\sqrt{\frac{2l+1}{2}\frac{(l-m)!}{(l+m)!}}P_{l'm'}(\cos\theta)\,P_{lm}(\cos\theta)\frac{e^{-im'\phi}}{\sqrt{2\pi}}\frac{e^{im\phi}}{\sqrt{2\pi}}\sin\theta\,d\theta\,d\phi$$
$$=\sqrt{\frac{2l'+1}{2}\frac{(l'-m')!}{(l'+m')!}}\sqrt{\frac{2l+1}{2}\frac{(l-m)!}{(l+m)!}}\left(\int_0^{\pi}P_{l'm}(\cos\theta)\,P_{lm}(\cos\theta)\sin\theta\,d\theta\right)\frac{1}{2\pi}\underbrace{\int_0^{2\pi}e^{im'\phi}e^{-im\phi}\,d\phi}_{=0\text{ for }m'\neq m} \tag{79}$$
$$=0.$$

(79) tells us that any two spherical harmonics with different $m$ values are orthogonal.

For the same $m$ and $l$

$$\int_0^{2\pi}\int_0^{\pi} Y_{lm}^*(\theta,\phi)\,Y_{lm}(\theta,\phi)\sin\theta\,d\theta\,d\phi \qquad (m \text{ and } l \text{ the same, no sum on them})$$
$$=\int_0^{2\pi}\int_0^{\pi}\sqrt{\frac{2l+1}{2}\frac{(l-m)!}{(l+m)!}}P_{lm}(\cos\theta)\,P_{lm}(\cos\theta)\frac{e^{im\phi}}{\sqrt{2\pi}}\frac{e^{im\phi}}{\sqrt{2\pi}}\sin\theta\,d\theta\,d\phi$$
$$=\sqrt{\frac{2l+1}{2}\frac{(l-m)!}{(l+m)!}}\underbrace{\left(\int_0^{\pi}P_{l'm}(\cos\theta)\,P_{lm}(\cos\theta)\sin\theta\,d\theta\right)}_{\sqrt{\frac{2}{2l+1}\frac{(l+m)!}{(l-m)!}}}\underbrace{\frac{1}{2\pi}\int_0^{2\pi}e^{im\phi}e^{-im\phi}\,d\phi}_{=1} \tag{80}$$
$$=1.$$

(80) tells us that the inner product of a spherical harmonic with itself equals one. This is our normalization for spherical harmonics.

Bottom line: Two spherical harmonics are orthogonal (inner product over a spherical surface is zero) unless both have the same $l$ and $m$. In that case the normalization is given by (81) with $m' = m$ and $l' = l$.

$$\int_0^{2\pi}\int_0^{\pi} Y_{l'm'}^*(\theta,\phi)\,Y_{lm}(\theta,\phi)\sin\theta\,d\theta\,d\phi=\delta_{ll'}\delta_{m'm} \qquad \text{Spherical harmonics orthonormality condition} \tag{81}$$

## 15.5 Visualizing Spherical Harmonics

Spherical harmonics are, generally, complex numbers, so it is difficult to convey their form on a 2D sheet. Not only are we sublimating 3D into 2D by so doing, but, more limiting, complex numbers comprise two real numbers, so we can't simply represent them with single real numbers (such as the $y$ value of $y = A \sin x$ on $x$-$y$ axes, or the radius from the origin to a surface in 3D).

Thus, in each diagram of Fig. A-3, we show the absolute value of the spherical harmonic as the distance from the origin to the surface shown, for the $l = 0,1,2$ cases. These values vary with direction in space pointing outward from the origin (except for $Y_{00}$, which is a sphere), as would be expected.

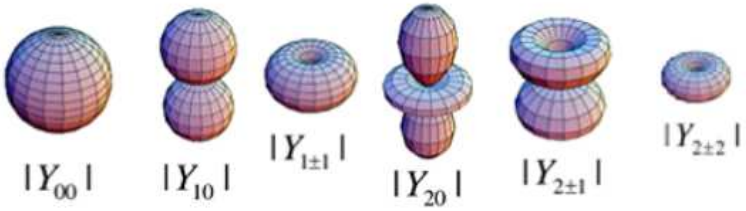


**Figure A-3. Absolute Values of Spherical Harmonics for $l = 0,1,2$ (Radial Length from Origin is Absolute Value of Spherical Harmonic)**

We can obtain real numbers with appropriate combinations of complex spherical harmonics, which, of course, is what we do for the CMBR, which is comprised of waves with real number (temperature) amplitudes.

## 15.6 Expanding a Function of $\theta$ and $\phi$ in $Y_{lm}$

### 15.6.1 The Expansion

Since the spherical harmonics are complete, we can expand any smooth function $f(\theta,\phi)$ in terms of them.

$$\boxed{f(\theta,\phi)=\sum_{l=0}^{\infty}\sum_{m=-l}^{l}a_{lm}Y_{lm}(\theta,\phi)}\,. \tag{82}$$

Noting that

$$\begin{aligned}\int_0^{2\pi}\int_0^{\pi}Y^*_{l'm'}(\theta,\phi)f(\theta,\phi)\sin\theta\,d\theta\,d\phi&=\int_0^{2\pi}\int_0^{\pi}Y^*_{l'm'}(\theta,\phi)\left(\sum_{l=0}^{\infty}\sum_{m=-l}^{l}a_{lm}Y_{lm}(\theta,\phi)\right)\sin\theta\,d\theta\,d\phi\\&=\sum_{l=0}^{\infty}\sum_{m=-l}^{l}a_{lm}\int_0^{2\pi}\int_0^{\pi}Y^*_{l'm'}(\theta,\phi)Y_{lm}(\theta,\phi)\sin\theta\,d\theta\,d\phi=\sum_{l=0}^{\infty}\sum_{m=-l}^{l}a_{lm}\delta_{ll'}\delta_{m'm}=a_{l'm'},\end{aligned} \tag{83}$$

we realize that we can find all $a_{lm}$ for any $f(\theta,\phi)$ via

$$\boxed{a_{lm}=\int_0^{2\pi}\int_0^{\pi}Y^{\dagger}{}_{lm}(\theta,\phi)f(\theta,\phi)\sin\theta\,d\theta\,d\phi.} \tag{84}$$

### 15.6.2 Note for $m\to -m$

Note from (68),

$$P_{l-m}=(-1)^m\frac{(l-m)!}{(l+m)!}P_{lm}\,. \tag{85}$$

Using (77) with $m\to -m$, incorporating (85), and recalling that $P_{lm}$ is real, we find

$$\begin{aligned}Y_{l-m}(\theta,\phi)&=\sqrt{\frac{2l+1}{2}\frac{(l+m)!}{(l-m)!}}\;P_{l-m}(\cos\theta)\frac{e^{-im\phi}}{\sqrt{2\pi}}\qquad\text{no sum on } l \text{ or } m\\&=\sqrt{\frac{2l+1}{2}\frac{(l+m)!}{(l-m)!}}\;(-1)^m\frac{(l-m)!}{(l+m)!}P_{lm}(\cos\theta)\frac{e^{-im\phi}}{\sqrt{2\pi}}=(-1)^m\sqrt{\frac{2l+1}{2}\frac{(l-m)!}{(l+m)!}}\;P_{lm}(\cos\theta)\frac{e^{-im\phi}}{\sqrt{2\pi}}\\&=(-1)^m\,Y^*_{lm}(\theta,\phi).\end{aligned} \tag{86}$$

### 15.6.3 Ramifications of $m\to -m$ Result

In our summation (82), for every spherical harmonic term $a_{lm}Y_{lm}$ there is a corresponding term

$$a_{l-m}Y_{l-m}=(-1)^m\,a^*_{l-m}Y^*_{lm}\,. \tag{87}$$

So, with appropriate choice of relation between $a_{lm}$ and $a_{l-m}$, i.e.,

$$a_{lm}=(-1)^m\,a^*_{l-m}=\text{ real number}\,, \tag{88}$$

the $m$ and $-m$ terms summed would be real for a given $l$. That is,

$$a_{lm}Y_{lm} + a_{l-m}Y_{l-m} = a_{lm}Y_{lm} + \underbrace{(-1)^m a_{l-m}^*}_{a_{lm}} Y_{lm}^* = a_{lm}\left(Y_{lm} + Y_{lm}^*\right) = \text{real function} \qquad (\text{no sum on } l \text{ or } m). \tag{89}$$

Also, for $m = 0$, $Y_{l0}$ is real. See (77) and recognize that $P_{lm}$ is real for any $m$.

Bottom line: $f$ in (82) can represent a real number (such as temperature of the CMB) even though the $Y_{lm}$ are complex.

### 15.6.4 Comparing to Fourier Analysis in the Cartesian Case

We can compare the representation of a function of $\theta$ in terms of a series of associated Legendre polynomials to the representation of a function of the Cartesian coordinate $x$ in terms of as series of sines and/or cosines (or equivalently, the real and/or imaginary part of $e^{ikx}$). Before doing so, we recall some trigonometric relations we will use along the way.

$$\sin^2\theta = \tfrac{1}{2}(1-\cos 2\theta) \quad (a) \qquad \cos^2\theta = \tfrac{1}{2}(1+\cos 2\theta) \quad (b) \qquad \sin\theta\cos\theta = \tfrac{1}{2}(\sin 2\theta) \quad (c) \tag{90}$$

$$\begin{aligned} &\sin^3\theta = \tfrac{1}{4}(3\sin\theta - \sin 3\theta) \quad (a) \qquad \cos^3\theta = \tfrac{1}{4}(3\cos\theta + \cos 3\theta) \quad (b) \\ &\cos\theta\cos 2\theta = \tfrac{1}{2}(\cos\theta + \cos 3\theta) \quad (c) \qquad \sin\theta\cos 2\theta = \tfrac{1}{2}(\sin 3\theta - \sin\theta) \quad (d) \end{aligned} \tag{91}$$

Now take (82) with $\phi = 0$, i.e., consider $f = f(\theta)$, and insert (77).

$$f(\theta) = \sum_{l=0}^{\infty}\sum_{m=-l}^{l} a_{lm}Y_{lm}(\theta,\phi=0) = \sum_{l=0}^{\infty}\sum_{m=-l}^{l} \underbrace{a_{lm}\sqrt{\frac{2l+1}{2}\frac{(l-m)!}{(l+m)!}}}_{a'_{lm}} P_{lm}(\cos\theta) = \sum_{l=0}^{\infty}\sum_{m=-l}^{l} a'_{lm}\, P_{lm}(\cos\theta)\ . \tag{92}$$

Compare this to a typical Fourier series expression for a function $h(x)$,

$$h(x) = \sum_{n=0}^{\infty} \left(a_n \cos nx + b_n \sin nx\right) \tag{93}$$

Now look at (68) (repeated below for convenience) to see what some of the associated Legendre polynomials used in (92) look like.

$$\begin{aligned} &P_{00} = 1 \qquad P_{10} = \cos\theta \qquad P_{20} = \frac{1}{2}\left(3\cos^2\theta - 1\right) \qquad P_{30} = \frac{1}{2}\cos\theta\left(5\cos^2\theta - 3\right) \\ &\qquad\qquad P_{11} = -\sin\theta \qquad P_{21} = -3\sin\theta\cos\theta \qquad P_{31} = -\frac{3}{2}\sin\theta\left(5\cos^2\theta - 1\right) \\ &\qquad\qquad\qquad\qquad P_{22} = 3\sin^2\theta \qquad P_{32} = 15\cos\theta\sin^2\theta \\ &\qquad\qquad\qquad\qquad\qquad\qquad P_{33} = -15\sin^3\theta \end{aligned} \tag{68}$$

where $P_{l-m} = (-1)^m \dfrac{(l-m)!}{(l+m)!} P_{lm}$ .

We then convert (68) using (90) and (91) to get

$$\begin{aligned} &P_{00} = 1 \qquad P_{10} = \cos\theta \qquad P_{20} = \tfrac{1}{2}\left(3\cos^2\theta - 1\right) = \tfrac{1}{2}\left(3\left(\tfrac{1}{2}(1+\cos 2\theta)\right) - 1\right) = \tfrac{1}{4} + \tfrac{3}{4}\cos 2\theta \\ &\qquad\qquad P_{11} = -\sin\theta \qquad P_{21} = -3\sin\theta\cos\theta = -\tfrac{3}{2}(\sin 2\theta) \\ &\qquad\qquad\qquad\qquad P_{22} = 3\sin^2\theta = \tfrac{3}{2} - \tfrac{3}{2}\cos 2\theta \end{aligned} \tag{94}$$

$$P_{30} = \tfrac{1}{2}\cos\theta\left(5\cos^2\theta - 3\right) = \tfrac{1}{2}\cos\theta\left(5\left(\tfrac{1}{2}(1+\cos 2\theta)\right) - 3\right) = -\tfrac{7}{4}\cos\theta + \tfrac{5}{4}\cos\theta\cos 2\theta$$
$$= -\tfrac{14}{8}\cos\theta + \tfrac{5}{8}(\cos\theta + \cos 3\theta) == -\tfrac{9}{8}\cos\theta + \tfrac{5}{8}\cos 3\theta$$

$P_{31}, P_{32}, P_{33}$ similarly yield expressions in $\cos\theta$, $\sin\theta$, $\cos 3\theta$, and $\sin 3\theta$.

The point is that terms in $\underline{P_{lm}}$ of order $l$ have highest order exponents in both sine and cosine factors combined of $l$ as shown in (68). These can be converted, as shown in (94), into expressions having terms with only sine and/or cosine of angles $l\theta$ ($l$ times $\theta$) not raised to any power. But those are exactly the kinds of terms we find in (93), for $l \to n$ and $\theta \to x$.

In essence, the summation (92) is the same summation as (93). For example, for the $a_3 \cos 3x$ term in (93), we would have a comparable term in (92) $c_3 \cos 3\theta$, where the $c_3$ is a combination of different $a_{lm}$. Each term in (93) has a corresponding term (when we add together all the appropriate $a_{lm}$ in the right way) in (92).

Bottom Line: The sum of all spherical harmonics in $\theta$ to yield a given function is effectively the same thing as a Fourier series summation of sines and cosines to yield the same function.

2nd Bottom Line: From (94), we see that the order $l$ of a spherical harmonic indicates the number of oscillations (in space across a constant radius sphere) from $\theta = 0$ to $\pi$, just as the order $n$ of a term in a Fourier analysis indicates the number of oscillations over the given interval from $x = 0$ to $L$.

Higher $n$ means more wavelengths inside $L$. Higher $l$ means more "wavelengths" inside 0 to $\pi$. (We use quotes on "wavelengths" in the spherical case, because (as we can see from the $l = 3$ case in (94)) a given $l$ harmonic includes sub waves that oscillate less rapidly (e.g., the $l = 3$, $m = 0$ case of (94) has both a $\cos 3\theta$ and a $\cos\theta$ term, not just a $\cos 3\theta$ term).

Question. So, one might ask, if we could use either the complicated spherical harmonics or the simpler sines and cosines, why not analyze a spherical surface, like the LSS (last scattering surface) using the latter, rather than the former?

Answer. I believe it is for the following reasons, the most foundational probably #4.

1. We can convert readily between Fourier harmonic components in Cartesian coordinates (used to deduce conclusions about plane waves from inflation, etc.) and spherical harmonic components in spherical coordinates (in which our measurements are done) via the methodology of Sect. 7.3, pg. 9.

2. It is conventional.

3. Spherical harmonics are used elsewhere in physics, particularly in QM for the hydrogen atom wave function, and physicists are familiar with them. In the H atom case, we had no real choice but to use spherical harmonics, because they are eigenfunctions of the Schrödinger equation with the isotropic potential energy of the Coulomb potential of the nucleus. The eigenvalues of $Y_{lm}$ are $m$ and $l$ (actually $l(l+1)$), which gave us respectively, the $z$ direction angular momentum and the square of total angular momentum.

4. Spherical harmonics are part of the solution set to the wave equation in spherical coordinates (as we saw before).

5. Spherical harmonics are eigenfunctions of any system having isotropic $g(\mathbf{x})$ in a governing equation like (57) (and the Schrödinger equation for the H atom). Since one of the foundational postulates of modern cosmology is isotropy, in the long run, it should prove advantageous to represent quantities of interest in the universe (like wave patterns in the LSS) via eigenfunctions to equation (57) with isotropic $g = g(r)$.

This would be particularly relevant for other cases involving 3D (unlike the 2D spherical surface of constant radius of the LSS). In such cases, we would have a non-trivial equation in $r$ (see (62)), which is an eigenvalue problem with eigenvalue $l(l + 1)$. Thus, for each $l$ (denoting a given eigenfunctions of $r$), there is a related eigenfunction of $\theta$, $\underline{P_{lm}}$ (for given $m$). However, any given sine or cosine function, such as $\cos 3\theta$, is *not* an eigenfunction for given $l$.

So, if we want to have the advantages of working in an eigenfunction basis for 3D isotropic cases, we need to use spherical harmonics, not sine/cosine functions.

### 15.6.5 An Example: A Dipole

Given that we align our spherical coordinate system (See Fig. A-2, pg. 29) in a given direction (say the $z$ axis is aligned perpendicular to the plane of the galactic disk). One might realize that if there were a particular multipole with respect to $\theta$ (particular $l$ value) aligned with a node right on the $z$ axis, then we could readily determine a suitable $a_{lm}$.

For example, consider the dipole of Fig. A-4, part a), aligned with the $z$ axis. It is described, at least in large part, by a temperature variation with $\theta$ of $\cos\theta$. Note from (77), and (82),

$$T(\theta,\phi) = f(\theta,\phi) = \sum_{l=0}^{\infty} \sum_{m=-l}^{l} a_{lm} Y_{lm}(\theta,\phi) == \sum_{l=0}^{\infty} \sum_{m=-l}^{l} a_{lm} \sqrt{\frac{2l+1}{2} \frac{(l-m)!}{(l+m)!}}\, P_{lm}(\cos\theta) e^{im\phi} . \tag{95}$$

From (68), we see the $l = 1$ terms include

$$P_{10} = \cos\theta \qquad P_{11} = -\sin\theta \qquad P_{1-1} = \frac{1}{2}\sin\theta \ . \tag{96}$$

Higher order ($l > 1$) terms represent higher multipoles and $l = 0$ represents a constant (no multipole) value of temperature with respect to $\theta$ equal to 2.725°K for the CMB (see dashed circle in Fig. A-4). So we would expect the $P_{10}$ term in the summation (95) to reflect the dipole of Fig. A-4a), i.e., $a_{10}$ would be much larger than any other $a_{lm}$.

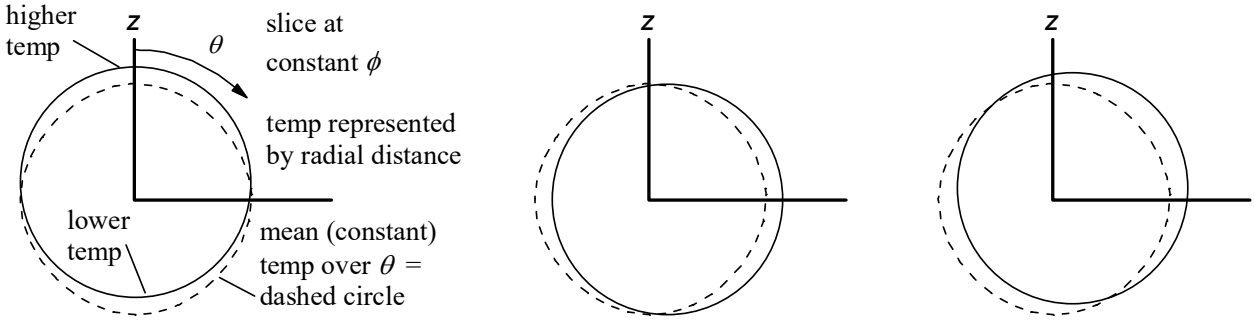


a) Aligned with $z$ axis, $|a_{10}|$ >> other amplitudes

b) Perpendicular to $z$ axis, $|a_{11}|$ and $|a_{1\text{-}1}|$ >> $|a_{10}|$

c) Aligned with some $\theta$ in between, all $a_{lm}$ significant

**Figure A-4. Temperature Dipole Aligned in Three Different Directions**

Similarly, in Fig. A-4b), the dipole is aligned such that the temperature variation, at least in large part, is described by $\sin\theta$. Thus, in that case, $P_{11}$ and $P_{1-1}$ would be the dominant contributing modes, with $a_{11}$ and $a_{1-1}$ being much larger than $a_{10}$. For the case of Fig. A-4c), we would have significant contributions from all three $P_{lm}$.

We now derive the $a_{lm}$ for each of the cases in Fig. A-4 and see if our intuitive statements above regarding them are correct. To do this, we first note what the $l = 1$ part of the spherical harmonics summation looks like in general, where we look only at the slice where $\phi = 0$, to keep things simple for now.

General Relation for Dipole with Any Alignment

$$T_{l=1}(\theta,\phi) = \sum_{m=-1}^{1} a_{1m} Y_{1m}(\theta,\phi) = \sum_{m=-1}^{1} a_{1m} \sqrt{\frac{2+1}{2}\frac{(1-m)!}{(1+m)!}}\, P_{1m}(\cos\theta) \underbrace{e^{im\phi}}_{\substack{\text{take}\\ \phi=0}}$$

$$= a_{10}\sqrt{\frac{3}{2}\frac{(1)!}{(1)!}}\cos\theta - a_{11}\sqrt{\frac{3}{2}\frac{(0)!}{(2)!}}\sin\theta + a_{1-1}\sqrt{\frac{3}{2}\frac{(2)!}{(0)!}}\frac{1}{2}\sin\theta \qquad (97)$$

$$= a_{10}\sqrt{\frac{3}{2}}\cos\theta - a_{11}\frac{\sqrt{3}}{2}\sin\theta + a_{1-1}\frac{\sqrt{3}}{2}\sin\theta .$$

Case of Fig A-4 a)

For the first case in Fig. A-4, we have a simple cosine dependence on $\theta$,

$$T_{l=1}(\theta,\phi) = X\cos\theta \qquad X = \text{max difference from mean temp} . \qquad (98)$$

So, in (97), we readily see that

$$a_{10} = \sqrt{\frac{2}{3}}X \qquad a_{11} = 0 \qquad a_{1-1} = 0 . \qquad (99)$$

Case of Fig A-4 b)

For the second case in Fig. A-4, we have a simple sine dependence on $\theta$,

$$T_{l=1}(\theta,\phi) = X\sin\theta . \qquad (100)$$

The following satisfy (97) and are the $a_{lm}$ values for the dipole as shown in Fig. A-4b).

$$a_{10} = 0 \qquad a_{11} = -\sqrt{\frac{1}{3}}X \qquad a_{1-1} = \sqrt{\frac{1}{3}}X . \qquad (101)$$

So,

$$T_{l=1}(\theta,\phi) = (0)\sqrt{\frac{3}{2}}\cos\theta + \frac{X}{\sqrt{3}}\frac{\sqrt{3}}{2}\sin\theta + \frac{X}{\sqrt{3}}\frac{\sqrt{3}}{2}\sin\theta = X\sin\theta. \tag{102}$$

Case of Fig A-4 c)

For the third case of Fig. A-4, we have the following values, which we prove are correct below.

$$a_{10} = \frac{X}{\sqrt{3}} \qquad a_{11} = -\frac{X}{\sqrt{6}} \qquad a_{1-1} = \frac{X}{\sqrt{6}}, \tag{103}$$

Note that the solid line of Fig. A-4c) is described by $X\sin(\theta + 45^{\circ})$. From the trig relation

$$\sin(\alpha \pm \beta) = \sin\alpha\cos\beta \pm \cos\alpha\sin\beta \qquad \text{with } \alpha = \theta \text{ and } \beta = 45^{\circ}, \tag{104}$$

$$X\sin(\theta + 45^{\circ}) = X(\sin\theta\cos 45^{\circ} + \cos\theta\sin 45^{\circ}) = \frac{X}{\sqrt{2}}\sin\theta + \frac{X}{\sqrt{2}}\cos\theta. \tag{105}$$

Using our stated values for the $a_{lm}$ from (103) in (97), we see it equals (105). That is,

$$T_{l=1}(\theta,\phi) = \frac{X}{\sqrt{3}}\sqrt{\frac{3}{2}}\cos\theta + \frac{X}{\sqrt{6}}\frac{\sqrt{3}}{2}\sin\theta + \frac{X}{\sqrt{6}}\frac{\sqrt{3}}{2}\sin\theta = \frac{X}{\sqrt{2}}\sin\theta + \frac{X}{\sqrt{2}}\cos\theta, \tag{106}$$

A Comment

I've tried to make this simple for illustrative purposes, but the astute reader may have noticed that the $a_{11}$ and $a_{1-1}$ are not uniquely defined above. Any of an infinite number of combinations of them could make (97) equal to (100) in Case b), or to (105) in Case c). Had we not limited this case to $\phi = 0$, in order to keep things simple, we could have shown they were actually unique for the more general case. See Sect. 15.6.3 pg. 35, where we show that, in general, for $T$ to be real (not complex), we must have $a_{l-m} = (-1)^m a_{lm}^* = \text{real}$. This is a further constraint that pins down the $a_{11}$ and $a_{1-1}$ values. Note that (101) and (103) obey this constraint.

### 15.6.6 Other Multipoles

In similar fashion for a sole higher multipole (more spatial oscillations in temperature with $\theta$ = more "highs" and "lows" = more nodes = higher $l$ value = $l'$, for this example), the values for $a_{l'm}$ in the $l'$ case would dominate over the $a_{lm}$ values for other $l$.

In a general case with many multipoles superimposed (as in the CMB), we get a spectrum of $a_{lm}$, the values for each $l$ and $m$ reflecting how strong that particular mode is relative to all others in the summation (95).

The difficult thing about spherical harmonics, as seen by the examples of (68), is that it is not easy to visualize the various modes and what physically, exactly, their amplitudes $a_{lm}$ represent. For a Fourier series like (93), we can envision what each mode looks like, and even draw figures representing the summations of the various modes. For spherical harmonics, on the other hand, this is problematic.

### *15.6.7* Angular Separation and *l*

From Fig. 6-A, pg. 38, one can see that for $l$ = 1, there are 180° degrees between nodes, i.e., there is a single variation ("bump", as it were) over the range of $0 \le \theta \le \pi$. For $l$ = 2, (think variation over $2\theta$, as in (94)) we would have three nodes (and two "bumps"), making a single variation (one "bump") over 90° degrees. For $l$ = 3 (variation over $3\theta$ as in (94)) we would have four nodes (three "bumps"), and a single variation (one "bump") over 60°. We can readily generalize to

$$\text{angular variation} = \frac{180^{\circ}}{l} \qquad \left(= \frac{\pi}{l} \text{ in radians}\right). \tag{107}$$

## 16 Appendix B. Introduction to Power Spectral Analysis

### 16.1 The Basis in Electronics for Power Considerations

Consider instantaneous power in an electric circuit

$$P_{inst} = VI, \tag{108}$$

where, for charge $q(t)$ a sinusoid, $\omega$ the frequency in radians/sec, and for simplicity impedance $Z$ = pure resistance $R$,

$$\begin{aligned} q(t) &= A\sin\omega t \qquad \left(A = q_{peak}\right) \\ I = \dot{q}(t) &= \omega A\cos\omega t \qquad V = RI = R\omega A\cos\omega t \end{aligned} \quad . \tag{109}$$

Thus, instantaneous power (108) is

$$P_{inst} = VI = R\omega^2 A^2 \cos^2\omega t = P_{peak}\cos^2\omega t \qquad P_{peak} = R\omega^2 A^2 \qquad \left(A = q_{peak}\right). \tag{110}$$

Since, for $T = 1/f = 2\pi/\omega$ the period of the oscillation,

$$\begin{aligned} &\text{variance of } q = \frac{1}{T}\int_0^T \left(q(t)\right)^2 dt = \frac{1}{T}\int_0^T A^2\sin^2\omega t\, dt = \frac{1}{T}\int_0^T A^2\left(\sin\frac{2\pi}{T}t\right)^2 dt = \frac{1}{T}\int_0^T A^2\left(cos\frac{2\pi}{T}t\right)^2 dt = \frac{A^2}{2} \\ &\text{standard deviation of } q = \sqrt{\text{variance}} = \text{rms value of } q = q_{rms} = \frac{A}{\sqrt{2}}, \end{aligned} \tag{111}$$

the average power (time average of the instantaneous power) is

$$\begin{aligned} &\underbrace{P = P_{mean}}_{\text{symbol def}} = \frac{1}{T}\int_0^T P_{inst}\, dt = \frac{1}{T}\int_0^T \underbrace{R\omega^2 A^2}_{P_{peak}} cos^2\omega t\, dt = \frac{P_{peak}}{2} = R\omega^2\frac{A^2}{2} \\ &\frac{A^2}{2} \text{ is variance of } q(t) \quad \left(A = q_{peak}\right) \end{aligned} \quad . \tag{112}$$

The point is the average power $P$ is proportional to $\omega^2$ times the amplitude of the peak charge squared $A^2$.

Now, for $q(t)$ a more general shape (non-sinusoid), we can find the Fourier components of $q$, which when added together (or integrated in the continuous case), give us $q(t)$. The amplitude of each such component is, in general, different at each value of $\omega$, so we label such amplitudes as $A_n$ (discrete case) or $A(\omega)$ (continuous case). That is,

$$\begin{aligned} &q(t) = \sum_{n=0}^{\infty}\left(A_n\sin\omega_n t + B_n\cos\omega_n t\right) \quad \text{or} \quad q(t) = \int\left(A(\omega)\sin\omega t + B(\omega)\cos\omega t\right)dt \\ &\text{take } B_n = B(\omega) = 0 \text{ for simplicity}, \end{aligned} \tag{113}$$

where we take the cosine parts to be zero, for simplicity, though to be complete for handling any shape $q(t)$, they would need to be included.

So, we would, in general, find a different average power $P$ in (112) for each $\omega$, and we define

$$\begin{aligned} P_n &= \text{ mean power for } n\text{th Fourier component in discrete case} \\ P(\omega) &= \text{ mean power per unit } \omega \text{ at } \omega \text{ in continuous case}, \end{aligned} \tag{114}$$

In general, when people use the word "power" in the context of spectral analysis, they mean "mean power over a full cycle" as in (112) and (114), not instantaneous power, as in (110).

From (112), we can see that if our Fourier components $A_n$ (or $A(\omega)$) of $q(t)$ had the same $A_n$ (or $A(\omega)$) at each $\omega_n$ (or $\omega$), the $P_n$ data points (or the $P(\omega)$ curve) would rise quadratically with $\omega$. A plot of $P(\omega)/\omega^2$ vs $\omega$, on the other hand would be a straight line. See Fig. B-1.

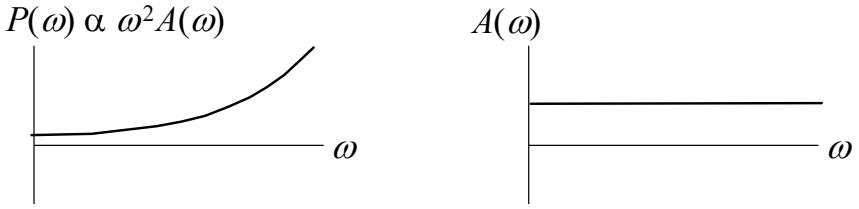


**Figure B-1. Constant Amplitude $A(\omega)$**

Intuitively, the behavior shown in Fig. B-1 could be expected. A sinusoidal wave of the same amplitude as another sinusoidal wave, but oscillating faster should have more power in it. Power depends on both the amplitude of the wave and the rate at which it oscillates.

White noise is defined as a straight line $P(\omega)$ vs $\omega$ curve, as shown in Fig. B-2 below. Each sinusoidal component at each $\omega$ has the same power density (power per unit $\omega$), but as can be seen in the RHS of the figure, different amplitude $A(\omega)$.

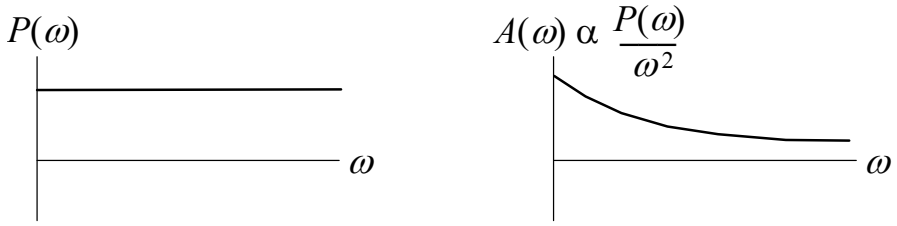


**Figure B-2. White Noise = Constant $P(\omega)$**

Fig. B-3 shows what white noise would look like in time, where the instantaneous contributions of every component of Fig. B-2 are summed as in (113) (actually, integrated for the continuous case of Fig. B-2) at each point in time.

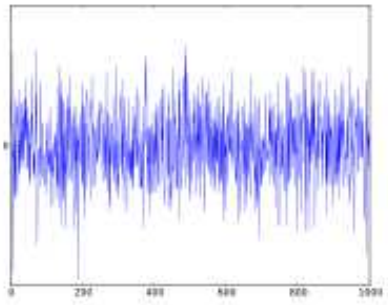

**Figure B-3. White Noise Instantaneous Power from All Components vs Time**

More general type systems show varying behaviors, with plots that are more complicated than the ones above, but the relationship

$$P(\omega) \propto \omega^2 \frac{\left(A(\omega)\right)^2}{2} \qquad A(\omega) = \text{amplitude of } \omega \text{ component wave} \qquad \frac{A(\omega)^2}{2} \text{ is variance of same wave} \tag{115}$$

always holds at each $\omega$ for any system.

## 16.2 Extrapolating to Other Types of Systems

The relations we developed in the prior section are commonly used for other fields outside of electronics. For spatially varying waves, for example, all of (108) to (114) can hold with different physical quantities, e.g.,

$$t \to x \qquad T \to \lambda \qquad q(t) \to S(x) \qquad \omega \to k \qquad A(\omega) \to A(k) \qquad P(\omega) \to P(k)$$
$$\lambda = \text{wavelength} \qquad S(x) = \text{ any function of } x \qquad k = \text{ wave number.} \tag{116}$$

For the CMB, we would take $S = T$, temperature (not period $T$ as the symbol was used for above). And thus, we can immediately deduce, in parallel with (112), that

$$P(k) \propto k^2 \frac{\left(A(k)\right)^2}{2} = k^2 \left\langle \left|A(k)\right|^2 \right\rangle$$
$$\frac{\left(A(k)\right)^2}{2} = \left\langle \left|A(k)\right|^2 \right\rangle \text{ is variance of } k \text{ wave component of temperature } T(x) \tag{117}$$
$$\left(A(k) = T_{peak} \text{ for } k \text{ component}\right).$$

In this case, $P(k)$ vs $k$ would be the temperature power spectrum. (Power is now being used in a more general, mathematical, sense, rather than being the kind of power one is accustomed to dealing with in mechanics and electronics. That is, power in the present sense does not have to be the time rate of change of work energy).

In the CMB analysis the above (Cartesian coordinates based) Fourier harmonics relationships are converted to (spherical coordinates based) spherical harmonics relationships, as shown in Sect. 10.

Note that units of $P(k)$ are power per unit $k$. When we integrate $P(k)$ over an interval $\Delta k$, we get the total power in that interval (a very useful relationship in many areas of physics and engineering).

$$\text{power between } k_1 \text{ and } k_2 = \int_{k_1}^{k_2} P\left(k\right) dk \tag{118}$$

Again, "power" in other contexts can mean something other than power as known in typical physics courses, and with other systems, such as that of (116), (118) holds with the surrogate symbols of (116) replacing those shown in (118).